



**UNIVERSIDADE ESTADUAL DE CAMPINAS
INSTITUTO DE QUÍMICA**

LUÍS ENRIQUE SANTA CRUZ HUAMANÍ

**MODULATION OF ELECTRONIC STRUCTURE OF RUTHENIUM(II)
TERPYRIDINE COMPLEXES BY COORDINATION TO HETEROARYL-2-
IMIDAZOLE LIGANDS**

**MODULAÇÃO DA ESTRUTURA ELETRÔNICA DE COMPLEXOS DE
RUTÊNIO(II) TERPIRIDINA ATRAVÉS DA COORDENAÇÃO AOS
LIGANTES HETEROARILO-2-IMIDAZOL**

**CAMPINAS
2016**

LUÍS ENRIQUE SANTA CRUZ HUAMANÍ

**MODULATION OF ELECTRONIC STRUCTURE OF RUTHENIUM(II)
TERPYRIDINE COMPLEXES BY COORDINATION TO HETEROARYL-2-
IMIDAZOLE LIGANDS**

**MODULAÇÃO DA ESTRUTURA ELETRÔNICA DE COMPLEXOS DE
RUTÊNIO(II) TERPIRIDINA ATRAVÉS DA COORDENAÇÃO AOS
LIGANTES HETEROARILO-2-IMIDAZOL**

Master's thesis presented to the Institute of Chemistry of the University of Campinas as part of the requirements to obtain the title Master's in Chemistry in the area of Inorganic Chemistry

Supervisor: Prof. Dr. André Luiz Barboza Formiga

**THIS COPY CORRESPONDS TO THE FINAL VERSION OF THE DISSERTATION
DEFENDED BY LUÍS ENRIQUE SANTA CRUZ HUAMANÍ AND SUPERVISED BY PROF.
DR. ANDRÉ LUIZ BARBOZA FORMIGA**

**CAMPINAS
2016**

Agência(s) de fomento e nº(s) de processo(s): CAPES

Ficha catalográfica
Universidade Estadual de Campinas
Biblioteca do Instituto de Química
Camila Barleta Fullin - CRB 8462

H874m Huamaní, Luis Enrique Santa Cruz, 1989-
Modulation of electronic structure of ruthenium(II) terpyridine complexes by coordination to heteroaryl-2-imidazole ligands / Luis Enrique Santa Cruz Huamaní. – Campinas, SP : [s.n.], 2016.

Orientador: André Luiz Barboza Formiga.
Dissertação (mestrado) – Universidade Estadual de Campinas, Instituto de Química.

1. Compostos de rutênio. 2. N-heterociclos. 3. Terpiridina. I. Formiga, André Luiz Barboza, 1978-. II. Universidade Estadual de Campinas. Instituto de Química. III. Título.

Informações para Biblioteca Digital

Título em outro idioma: Modulação da estrutura eletrônica de complexos de rutênio(II) terpiridina através da coordenação aos ligantes heteroarilo-2-imidazol

Palavras-chave em inglês:

Ruthenium compounds

N-heterocycles

Terpyridine

Área de concentração: Química Inorgânica

Titulação: Mestre em Química na área de Química Inorgânica

Banca examinadora:

André Luiz Barboza Formiga [Orientador]

Sofia Nikolaou

Juliano Alves Bonacin

Data de defesa: 01-08-2016

Programa de Pós-Graduação: Química

BANCA EXAMINADORA

Prof. Dr. André Luiz Barboza Formiga (Orientador)

Profa. Dra. Sofia Nikolaou (FFCLRP-USP)

Prof. Dr. Juliano Alves Bonacin (IQ-UNICAMP)

A Ata da defesa com as respectivas assinaturas dos membros encontra-se no processo de vida acadêmica do aluno.

Este exemplar corresponde à redação final da
Dissertação de Mestrado defendida pelo aluno **LUÍS
ENRIQUE SANTA CRUZ HUAMANÍ**, aprovada pela
Comissão Julgadora em 01 de agosto de 2016

Le dedico este trabajo a mis padres Santos Eliseo Santa Cruz Salazar y Fortunata Huamaní Cabrera, así como también a mi hermano Oscar Fernando Santa Cruz Huamaní, porque ellos son parte fundamental de todo lo que he logrado.

Acknowledgements

Agradeço aos meus pais pelo apoio incondicional em todas as etapas da minha vida, pelo carinho que eles me dão, pelos valiosos conselhos que eles me oferecem no dia a dia, pela total confiança que eles depositam em mim, pelas palavras de alento para não me abater nos momentos difíceis, pela paciência e sobre todo pelos valores que eles sempre me inculcam.

Agradeço ao meu irmão pela companhia que me deu em todas as minhas etapas, pelas trocas de ideias tão valiosas e sobre todo pelos momentos de alegria compartilhados.

Agradeço aos meus tios Domingo Huamaní, Salvador Santa Cruz e Nicolasa Lazo, bem como a minha madrinha Estrella Delzo, pelo apoio incondicional que me brindaram durante a grande parte da minha vida.

Agradeço aos meus amigos: Rocío Espinoza, pela valiosa amizade incondicional, momentos de muita alegria e conselhos; Katherine Romero, pelas conversas agradáveis; Javier Lobatón, pelo apoio oferecido em todo momento.

Agradeço ao Prof. Dr. André Formiga pela oportunidade brindada de trabalhar no seu grupo de pesquisa e permitir o meu crescimento na parte acadêmica.

Agradeço aos meus amigos do laboratório Kalil Toledo, por ter me ensinado a língua portuguesa de uma maneira muito “pedagógica” nos primeiros meses da minha estadia, pelos momentos de bom humor e pelas dicas relacionadas com o RMN. Ao Renan Guerra, pelos ensinamentos e dicas oferecidas, bem como as conversas sem sentido, mas muito engraçadas. Ao Douglas Nakahata, pela valiosa ajuda oferecida tanto no uso dos equipamentos quanto nas discussões. Ao Marcos Ribeiro, pelo convívio agradável, pela ajuda no uso de equipamentos e dicas relacionadas e as conversas tão interessantes sobre o futebol. À Vera Katic, pela ajuda brindada e a “grande alegria” que espalha pelo laboratório. À Ana Thereza Fiori pelo juízo racional, sensato e lúcido que dissipa em cada uma das suas palavras. À Naheed Bibi pelo esforço que faz dia a dia por entender o meu desastroso, triste e lamentável inglês. Ao Márcio Monteiro por razões de índole burocrática. Muito obrigado Pãmyla Santos, Bruno Morandi, Marcos Carvalho, Raphael Enoque, Julia Nunes, Fernando Bergamini, Augusto Firmino e Carlos Manzano pela companhia e ajuda. Gostaria de agradecer também à Cintia Saito pela ajuda tão valiosa que nos brinda e que facilita a nossa vida no laboratório.

Resumo

A modulação das estruturas eletrônicas dos complexos $[\text{RuCl}(\text{L})(\text{tpy})]^+$ foi avaliada. Para este propósito, diferentes ligantes heteroarilo-2-imidazol L {L: 2-(1H-imidazol-2-il)piridina (Himpy), 2-(1H-imidazol-2-il)pirazina (Himpz), 2-(1H-imidazol-2-il)pirimidina (Himpm) ou 3-(1H-imidazol-2-il)piridazina (Himpa)} foram usados. Os compostos $[\text{RuCl}(\text{L})(\text{tpy})]\text{PF}_6$ foram obtidos através da reação entre o complexo precursor $[\text{Ru}(\text{tpy})\text{Cl}_3]$ e os ligantes heteroarilo-2-imidazol (L) em etanol e usando trietilamina como agente redutor. A composição dos compostos foi determinada por análise elementar, além das medidas de condutividade em diferentes solventes. A espectroscopia de ressonância magnética nuclear (RMN- ^1H) foi usada para elucidar as estruturas dos ligantes e complexos. Após coordenação dos ligantes L, foram observadas novas bandas MLCT na região 400-600 nm. Cristais dos compostos $[\text{RuCl}(\text{Himpy})(\text{tpy})]\text{Cl}$ e $[\text{RuCl}(\text{Himpz})(\text{tpy})]\text{PF}_6$ foram obtidos a partir da evaporação lenta das soluções em acetonitrila. As estruturas cristalinas mostraram o ligante terpiridina na posição meridional, enquanto que o anel heteroarilo estava na posição cis ao ligante terpiridina. A voltametria cíclica mostrou todos os potenciais de oxidação dos complexos em torno de 0,3 V vs. o par redox Fc/Fc^+ , com o complexo $[\text{RuCl}(\text{Himpy})(\text{tpy})]^+$ exibindo o menor potencial de oxidação. Os espectros RMN- ^1H dos complexos $[\text{RuCl}(\text{L})(\text{tpy})]^+$ mostraram algumas impurezas que foram relacionadas aos seus isômeros, os quais apresentam o anel heteroarilo estando na posição trans ao anel terpiridina.

Abstract

The modulation of electronic structures of $[\text{RuCl}(\text{L})(\text{tpy})]^+$ complexes was evaluated. Different heteroaryl-2-imidazole ligands L {L: 2-(1H-imidazol-2-yl)pyridine (Himpy), 2-(1H-imidazol-2-yl)pyrazine (Himpz), 2-(1H-imidazol-2-yl)pyrimidine (Himpm) or 3-(1H-imidazol-2-yl)pyridazine (Himpa)} were used to this purpose. The compounds $[\text{RuCl}(\text{L})(\text{tpy})]\text{PF}_6$ were obtained through reaction of $[\text{Ru}(\text{tpy})\text{Cl}_3]$ complex and the heteroaryl-2-imidazole ligand (L) in ethanol and using triethylamine as a reducing agent. The composition of the compounds was determined by elemental analysis as well as by conductivity measurements in several solvents. Nuclear magnetic resonance spectroscopy ($^1\text{H-NMR}$) was used to elucidate the structures of the ligands and complexes. After coordination of L, new MLCT bands were observed in the 400-600 nm region. $[\text{RuCl}(\text{Himpy})(\text{tpy})]\text{Cl}$ and $[\text{RuCl}(\text{Himpz})(\text{tpy})]\text{PF}_6$ crystals were obtained from slow evaporation of the acetonitrile solutions. The X-ray structures showed the terpyridine in a meridional position, whereas the heteroaryl ring was in a cis position to terpyridine ring. Cyclic voltammetry displayed all the oxidation potentials around 0.3 V vs. Fc/Fc⁺ couple, with complex $[\text{RuCl}(\text{Himpy})(\text{tpy})]^+$ exhibiting the less positive oxidation potential. $[\text{RuCl}(\text{Himpy})(\text{tpy})]\text{Cl}$ and $[\text{RuCl}(\text{Himpz})(\text{tpy})]\text{PF}_6$ crystals were obtained from slow evaporation of the acetonitrile solutions. The $^1\text{H-NMR}$ spectra of the $[\text{RuCl}(\text{L})(\text{tpy})]^+$ complexes showed some impurities that were correlated to their isomer, which show pyridine ring in a trans position to terpyridine ring.

Abbreviations, Acronyms and Symbols

bpy	2,2'-bipyridine
CHCl ₃	Chloroform
CH ₂ Cl ₂	Dichloromethane
CH ₃ CN	Acetonitrile
CH ₃ COCH ₃	Acetone
CH ₃ OH	Methanol
C ₂ H ₅ OH	Ethanol
CNTs	Carbon nanotubes
COSY	Correlation Spectroscopy
DMF	Dimethylformamide
DMSO	Dimethylsulphoxide
ESI-MS	Electrospray Ionization Mass Spectrometry
Himpa	3-(1H-imidazol-2-yl)pyridazine
Himpn	2-(1H-imidazol-2-yl)pyrimidine
Himpy	2-(1H-imidazol-2-yl)pyridine
Himpz	2-(1H-imidazol-2-yl)pyrazine
HMBC	Heteronuclear Multiple Bond Correlation
HOMO	Highest Occupied Molecular Orbital
HSQC	Heteronuclear Single Quantum Correlation
LUMO	Lowest Unoccupied Molecular Orbital
MLCT	Metal to Ligand Charge Transfer
<i>mer</i>	Meridional
NH ₄ PF ₆	Ammonium hexafluorophosphate
NMR	Nuclear Magnetic Resonance
ORTEP	Oak Ridge Thermal Ellipsoid Plot
P4VP	Poly(4-vinylpyridine)
SWCNTs	Single Walled Carbon nanotubes
TBAPF ₆	Tetrabutylammonium hexafluorophosphate
TLC	Thin Layer Chromatography
tpy	2,2':6',2''-terpyridine

Summary

1. Introduction	11
1.1 Ruthenium(II) polypyridyl complexes.....	11
1.2 Terpyridyl complexes.....	11
1.4 Nitrogen-containing heterocycles	15
1.4 Modification of surface electrodes with redox polymers-functionalized carbon nanotubes	19
2. Aim	23
3. Experimental.....	24
3.1 Materials and measurements	24
Materials.....	24
Measurements	24
3.2 Preparation of films for conductivity measurements.....	25
3.3 Synthesis of [Ru(tpy)Cl ₃]	25
3.4 Synthesis of 3-(1H-imidazol-2-yl)pyridazine – Himpa.....	26
3.5 Synthesis of [RuCl(Himpy)(tpy)]Cl.....	26
3.6 Synthesis of [RuCl(Himpy)(tpy)]PF ₆	27
3.7 Synthesis of [RuCl(Himpa)(tpy)]PF ₆	28
3.8 Synthesis of [RuCl(Himpm)(tpy)]PF ₆	28
3.9 Synthesis of [RuCl(Himpz)(tpy)]PF ₆	28
4. Results and discussions	30
4.1 [Ru(tpy)Cl ₃] complex	30
4.2 3-(1H-imidazol-2-yl)pyridazine “Himpa”	32
4.3 Synthesis and characterization of [RuCl(L)(tpy)] ⁺ complexes	37
4.4 Mass spectrometry.....	37
4.5 ¹ H-NMR spectroscopy of Ru(II) complexes and their crystal structures	40
4.6 Electrochemistry of the complexes	51
4.7 Electronic properties of the complexes	53
4.8 Conductivity measurements of the films	56
5. Conclusions.....	57
6. References	58

1. Introduction

1.1 Ruthenium(II) polypyridyl complexes

Ruthenium(II) is a d^6 metal ion, whereas polypyridyl ligands are coordinating organic molecules having σ -donor properties due to lone pairs of nitrogen atoms, π -donor properties coming from π electron cloud-rich ring such as five-membered heterocycle imidazole as well as π^* -acceptor properties coming from π electron cloud-deficient ring such as six-membered heterocycle pyridine. Their complexes are characterized by usually displaying a distorted octahedral geometry, being them homoleptic complexes containing either bidentate or tridentate ligands, or heteroleptic complexes, showing an electronic absorption spectrum which consists of both ultraviolet region featuring absorption bands arising from $\pi \rightarrow \pi^*$ orbital transitions – ligand centered LC - (usually c.a. 240 nm and 300 nm) which arise from polypyridyl moiety, and a visible region (400 nm – 700 nm) showing $Ru(d\pi^6) \rightarrow \pi^*(\text{ligand})$ metal to ligand charge-transfer (MLCT) transitions, whose molar extinction coefficient is not so high as corresponding to ligand centered transitions and depend on ligand nature.¹

Since the early work of Demas and Crosby in 1971² concerned to luminescence quantum yields and lifetimes for several polypyridyl-containing Ru(II) complexes, many research works have been carried out related not only to the study of those physical properties, but also in applications such as in solar energy conversion as sensitizers.^{1,3-9} Furthermore, they exhibit catalytic capability of oxidizing water taking advantage of $Ru(IV)=O$ species formed through loss of four protons and four electrons from starting Ru(II) complex, which are needed for water splitting ($2H_2O \rightarrow O_2 + 4H^+ + 4e^-$).¹⁰ In addition, they can be used as electroactive groups in self-assembled monolayers for proton-coupled electron transfer reactions, which are important in biochemistry field.¹¹

1.2 Terpyridyl complexes

Among Ru(II) polypyridyl complexes, terpyridyl-containing complexes have shown remarkable photophysical and electrochemical properties.¹²⁻¹⁷ The polypyridyl molecule terpyridine was isolated for the first time in 1931, obtaining it as white crystals (m.p. 88-89°C) from dehydrogenation of pyridine by anhydrous ferric chloride.¹⁸ Despite that, only several years later that publications related to terpyridine started to appear.¹⁹⁻²⁵ The first publications concerned to the high stability

displayed after coordination to metals,²¹ its use as redox indicator after coordination to metals for spectrophotometric determinations of them,¹⁹ highlighting its behavior as an organic complexing agent.²⁰ As its importance in complexes was increasing, several studies emphasized the determination of several physical constants, specifically in spectrophotometric constants.^{20,21,24} Substitutions on terpyridine ring were performed in order to improve those constants, such as wavelengths of maximum absorption lying in the visible region as well as molar coefficient constant because of its direct relationship to sensitivity.^{24,25}

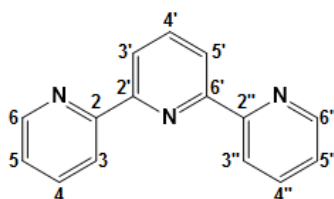


Figure 1: 2,2':6',2'' terpyridine ligand.

Ruthenium(II) terpyridyl complexes have been subject of study because of their outstanding physical, spectroscopic and reversible redox behavior. As mentioned for polypyridyl complexes, they exhibit characteristic LC bands due to $\pi \rightarrow \pi^*$ transitions as well as MLCT bands originated from $\text{Ru}(d\pi^6) \rightarrow \pi^*(\text{terpyridine})$. As they participate in electron transfer reactions in many areas, it is important for them to display reversible redox behavior, and that is usually assessed through use of cyclic voltammetry. In such a diagram obtained after performing the electrochemical measurements, the oxidation process occurs on the metal center of the complex, that is, electrons are removed from HOMO orbital (usually metal centered). This process requires energy that can be modulated provided that electron withdrawing or donating groups are present. Maestri and co-workers²⁶ carried out a systematic investigation on the effect of varying the substituents on 4'-position of terpyridine ligands in order to modify redox as well as luminescent properties. As expected, electron donating substituents such as OH^- , $\text{C}_2\text{H}_5\text{O}^-$, $(\text{CH}_3)_2\text{N}^-$ groups shifted cathodically the metal centered oxidation potentials, whereas electron withdrawing groups such as Cl^- , CH_3SO_2^- shifted them to more positive region. Even more, reduction potentials, which are related to LUMO energies, were shifted to more

negative values as electron donating groups were involved, whereas the opposite happened with electron withdrawing groups.

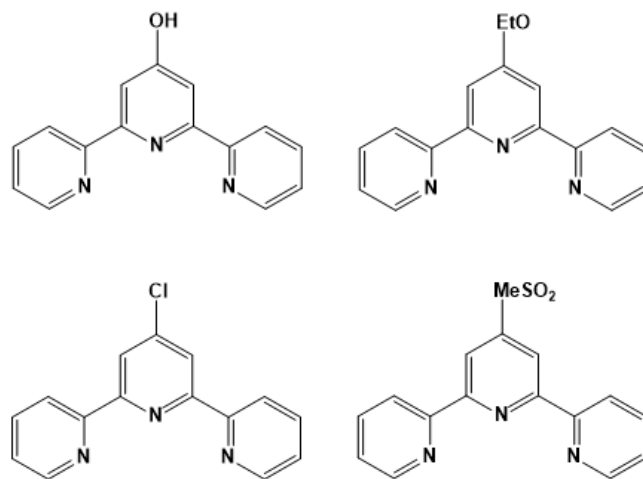


Figure 2: 4'-substituted terpyridine ligands. Adapted from Maestri et al.²⁶

The basicity strength of pyridyl substituents also influences on redox properties of Ru(II) terpyridine complexes. Introduction of pyrimidyl ring into 4' position of terpyridine ring did not alter significantly the oxidation potentials of ruthenium(II) complexes containing those ligands, while reduction potentials were shifted to a more anodic region. It was also displayed that substituents on pyrimidyl moiety influenced the reduction potentials, as expected from electronic density dependence. Those results showed that was possible to tune LUMO energies without modifying oxidation potentials of the metal center.²⁷

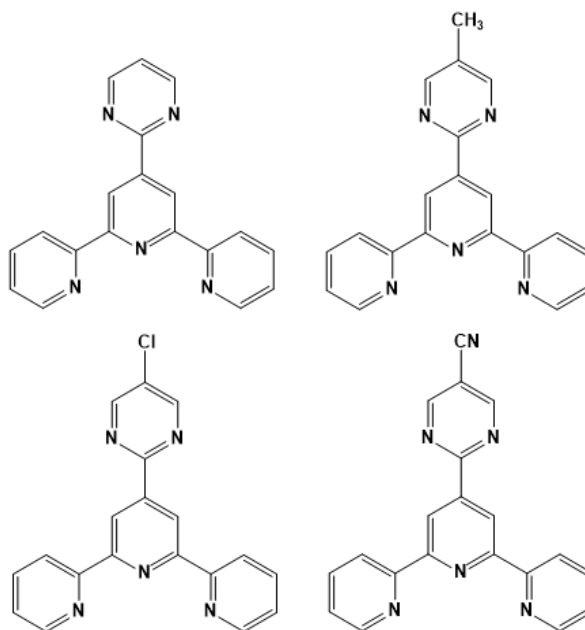


Figure 3: 4'-pyrimidyl-substituted terpyridine ligands. Adapted from Fang et al.²⁷

Contrary to $[\text{Ru}(\text{bpy})_3]^{2+}$, which exhibits intense room temperature luminescence and long excited-state lifetime,² $[\text{Ru}(\text{tpy})_2]^{2+}$ complex is known not to display room temperature luminescence as well as a short excited-state lifetime (0.25 ns),²⁸ making it not a suitable compound for applications in light-induced processes. Those short excited-state lifetimes are likely to be due to the small energy gap between the excited triplet metal to ligand charge-transfer ($^3\text{MLCT}$) state and the excited triplet metal-centered (^3MC) state.¹ As a consequence, numerous research studies have been performed in order to increase that energy difference. That can be carried out by using electron donor or acceptor groups depending on the system to study.^{3,16,17,29} If it were used an electron withdrawing group, it would be expected a stabilization of π^* orbital, which in turn would increase the energy gap between $^3\text{MLCT}$ and ^3MC states (if ^3MC energy is higher than $^3\text{MLCT}$ energy), resulting in greater excited-state lifetime. Wang and co-workers³⁰ performed a study concerning the modification of terpyridine ring by substituting one hydrogen by a cyano group in 4'-position. Greater room temperature excited-state lifetimes as well as intense luminescence quantum yields were obtained, as probably the energy gap between the excited triplet states increased through use of the cyano group.

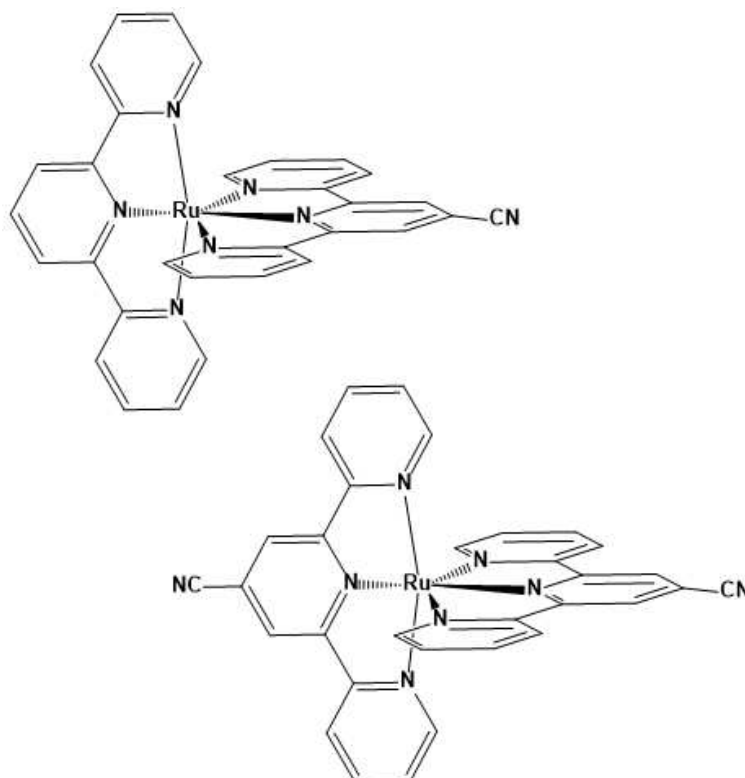


Figure 4: Ru(II) complexes containing cyano-terpyridine. Adapted from Wang et al.³⁰

More significant changes can be obtained as a result of replacing C-H groups by electronegative nitrogen atoms. Furthermore, changes in position of those nitrogen atoms can modify electron-withdrawing behavior. Such changes have a great influence on π donor/acceptor properties on aromatic heterocycles like pyridine.³¹ Six-membered nitrogen heterocycles compounds are excellent π -acceptors while five-membered heterocycles are much poorer π -acceptors and better π -donors. Those characteristics can have important consequences in spectral and redox properties of complexes containing them.

1.4 Nitrogen-containing heterocycles

These unsaturated organic compounds are characterized by possessing two different atoms in the ring, i.e., nitrogen atoms instead of CH- groups as well as the carbon atoms. Five-membered and six-membered systems are the most extensively studied because they occur in natural products, drugs, and also they are not only biologically but industrially important. Most known heterocyclic diimine compound 2,2'-bipyridine was synthesized by Blau in 1888,³² and since then, several

research investigations were carried out on complexes containing it because of the interesting redox and photophysical properties.^{1,33}

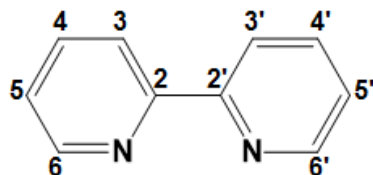


Figure 5: 2,2'-bipyridine ligand.

Such a high number of investigations concerning bipyridine and other N-heterocyclic ligands is because of the remarkable redox reversible behavior and photophysical properties exhibited in complexes containing it, specifically, in ruthenium(II) compounds.^{4,34–39}

N-heterocyclic compounds are so interesting because they can adopt a high diversity of structures, which in turn modifies their electronic, physical and redox properties. For example, N-heterocyclic diazines such as bipyrazine, bipyrimidine and bipyridazine have shown to display a weak strength basicity compared to bipyridine⁴⁰ (**Figure 6**).

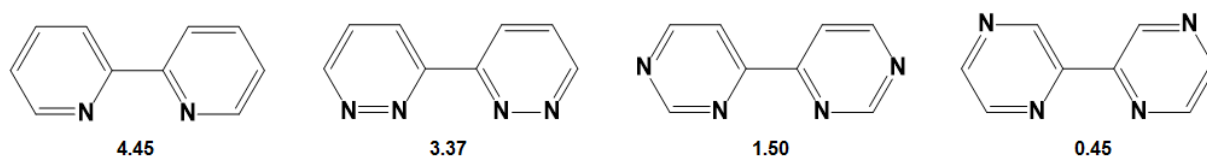


Figure 6: pK_a values for some diazine ligands.⁴¹

Depending on the position of the nitrogen atom in the structure, basicity strength of bidiazines changes and that characteristic is usually used for purposes such as altering the energy of maximum absorption in visible region for ruthenium complexes (MLCT energy), the energy needed for removing electrons from metal center (oxidation potential) and adding electrons to ligand (reduction potential). Such changes are strongly related to each other as for other Ru(II) polypyridyl complexes, since the HOMO is not only related to MLCT energies, but also with oxidation and reduction potentials.⁴² Those modifications have a great importance in many

applications including photocatalysis for solar energy conversion,^{43,44} electrochemical oxidative catalyst.⁴⁵

Diazadiimine ligands were reported⁴⁴ to shift anodically the oxidation potential of the ruthenium(II) complexes containing them with respect to $[\text{Ru}(\text{bpy})_3]^{2+}$, illustrating their weaker σ -donor behavior. One of those complexes, $[\text{Ru}(\text{bprid})]^{2+}$ (bprid = bipyridazine), showed to be a better photocatalyst than $[\text{Ru}(\text{bpy})_3]^{2+}$, featuring how properties can be modified by changing the six-membered ring. Ruthenium complexes were synthesized containing pyridin-2-yl-1,2,4-triazoles⁴⁶ in order to compare them to bipyridyl ligand. It was changed the pyridyl ligand by triazole ligand in order to investigate how would influence the donor-acceptor properties of triazole on electronic and electrochemical properties of those complexes. As expected, acceptor properties decreased compared to bipyridine ligand, according to more negative reduction potentials obtained. Oxidation potentials did not significantly change compared to bipyridine ligand (they appeared to be 10 mV less positive than of bpy).

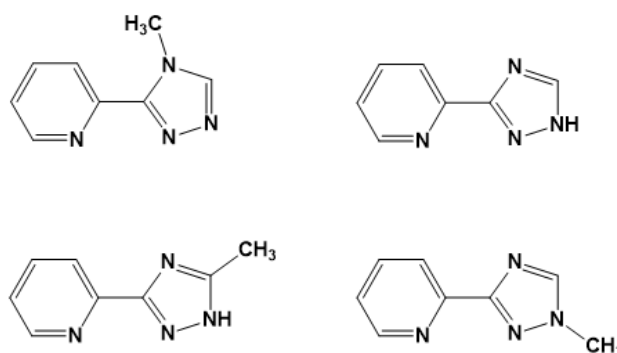


Figure 7: Pyridine-2-yl-1,2,4,-triazole ligands used in the synthesis of Ru(II) complexes. Adapted from Hage R. et al.⁴⁶

Complexes of deprotonated form of derivative bibenzimidazole ligands were reported by Haga.⁴⁷ That work showed that after deprotonation of the ligands, the oxidation potential of ruthenium center was shifted cathodically, highlighting the increasing of their π -donor properties. It was reported the synthesis of platinum(II) complexes containing bidiazine ligands, focusing on the strength of backdonation in the complexes through the use of MLCT energies. Specifically, 3,3'-bipyridazine (**5**), 3,6-bis(2'-pyridyl)pyridazine (**3**) were compared to bipyrazine (**4**), bipyrimidine (**2**), and bipyridine (**1**). It was found that the MLCT energies decreased in the order **1** > **2**

> **3** > **4** > **5** so based on those energies values, it was concluded that the strength of backdonation follows the reverse order.

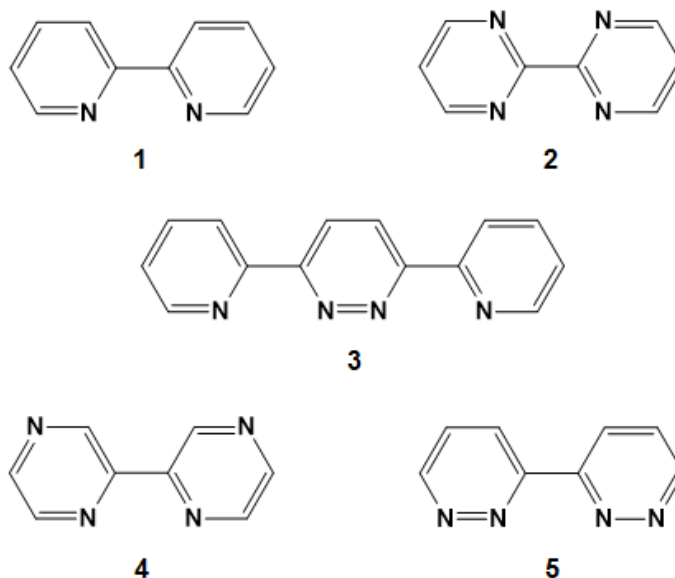


Figure 8: Bidiazine ligands. Adapted from Ghedini et al.⁴⁸

Bidiazine **4**, despite being a good π acceptor ligand, it has a poor sigma donor which lowers its ability to be involved in strong backbonding.⁴⁸ This behavior reflects how much the donor/acceptor properties of ligands could influence electronic and redox properties of complexes containing them. Ernst and Kaim studied⁴¹ the donor/acceptor influence of some bidiazine ligands (bipyridine **bpy**, bipyrazine **bpz**, bipyrimidine **bpym** and bipyridazine **bpdz**) on tungsten(0) complexes through MLCT energies, finding those charge-transfer energies decrease as follows: **bpy** > **bpym** > **bpz** > **bpdz**. Reduction potentials obtained were in agreement with LUMO energies of the complexes, except for **bpz** and **bpdz** ones. Although the former complex was found to have the lower reduction potential, it showed a higher charge-transfer energy than the latter complex. It was related to a higher basicity of **bpdz** ($pK_a = 3.37$) compared to **bpz** ($pK_a = 0.45$), which increases the HOMO energy of the complex.

Such a versatility in donor-acceptor properties of nitrogen-containing heterocycle ligands can be exploited in many areas such as water splitting catalysis,^{43,49} modification of surface electrodes,⁵⁰ photochemical molecular devices.⁵¹

1.4 Modification of surface electrodes with redox polymers-functionalized carbon nanotubes

Since the discovery of carbon nanotubes (CNTs) in 1991 by Iijima,⁵² they have received great interest principally because of their unique optical, adsorption, high electrical conductivity, mechanical characteristics and chemical stability.^{53–56} The mentioned features make them attractive for many applications, particularly in the development of electrochemical sensors.⁵⁷ Nevertheless, one of the problems to prepare electrochemical sensors based on CNTs is the low solubility thereof in most solvents.⁵⁸ Usual methods of CNTs functionalization use strong oxidizing agents, which can modify the structure of the CNTs and thus, change their electronic properties.^{59–61} For example,⁶² carboxylation of single-walled carbon nanotubes (SWCNTs) by nitric acid makes the photoconductivity of SWCNTs fairly difficult to be controlled. However, covalent attachment of $[\text{Ru}(\text{bpy})_3]^{2+}$ caused carbon nanotubes to be persistently photoconductive which could be used for many applications like for example as sensors.

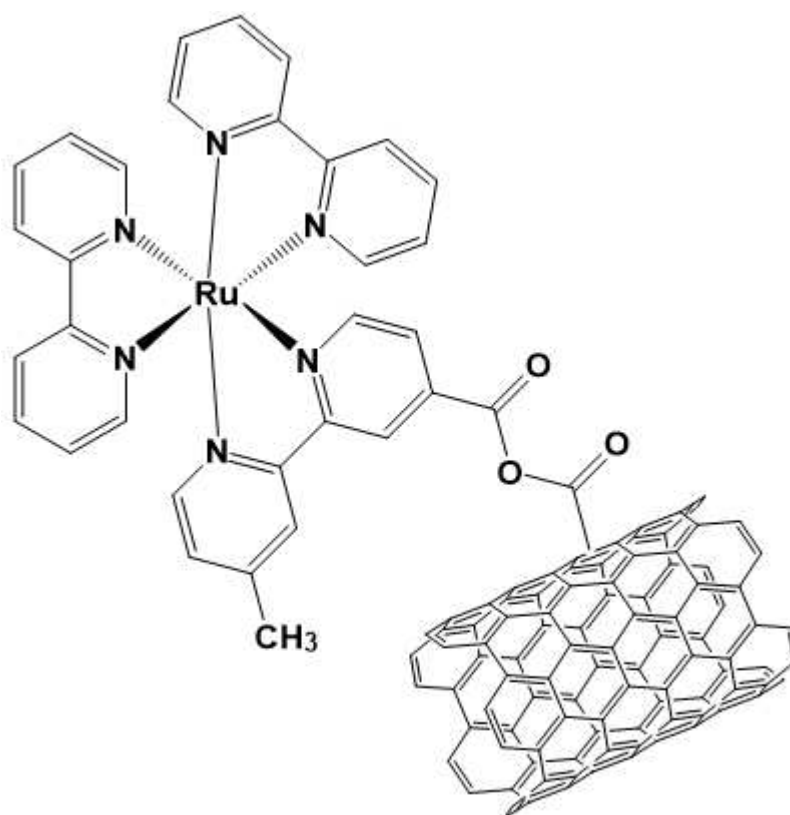


Figure 9: Chemically modified carbon nanotubes with $[\text{Ru}(\text{bpy})_3]^{2+}$. Adapted from Khairoutdinov et al.⁶²

In order to keep electronic properties, soft non-covalent functionalization methods are preferred instead of oxidizing ones (**Figure 10**).⁶³

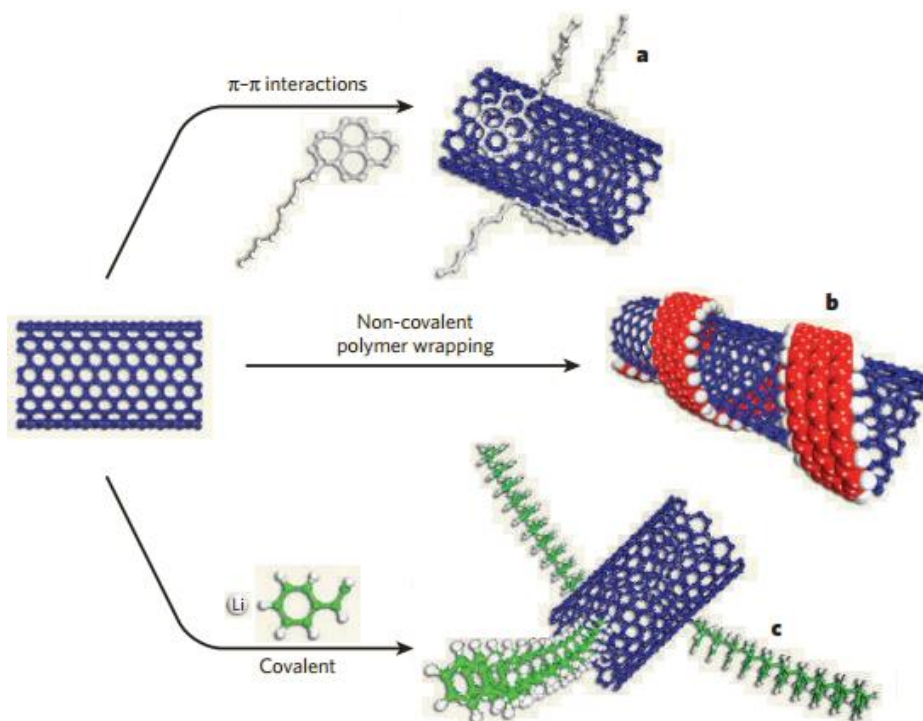


Figure 10: Strategies for stabilization of CNTs in solvents. a) Aromatic molecules can be appended to CNTs by using π - π interactions. Groups emanating from these molecules interact with the surrounded solvent or matrix. b) Non-covalent interactions (including van der Waals forces and charge-transfer interactions) can be used to wrap polymers around CNTs. c) Chemical groups can be covalently attached to the CNT.⁶³

One of these functionalization methods consist of wrapping polymers around the nanotubes surface through interactions such as van der Waals forces (Erro! Fonte de referência não encontrada. **b**). Modification with polymers is attractive since they can be assembled into homogeneous thin films, which makes them useful for electrochemical sensors development. Furthermore, the response displayed through use thereof is largely increased over other kind of processes such as the mentioned chemical functionalization, as well as the advantages in catalytic applications.⁶⁴ Earlier reports related to use of redox polymer systems dating back to 1979, where Oyama and Anson⁶⁵ reported the attachment of polyvinylpyridine with a ruthenium(II) complex to a graphite surface electrode. Redox metallopolymers such as that formed by P4VP bearing a coordination compound with known redox properties like ruthenium or osmium complexes⁶⁶ have long been used for electrode

modification. Modified electrodes with these metallopolymers bearing ruthenium polypyridine complexes show reversible surface-attached redox couple, strong catalytic properties, with the coatings being stable in several solvents.⁶⁷ Specifically, redox polymers were studied by Calvert and Meyer⁶⁸ using poly(4-vinylpyridine) (P4VP). They used the $[\text{Ru}(\text{OH}_2)(\text{tpy})(\text{bpy})]^{2+}$ complex for preparation of the metallopolymer and emphasize its usefulness by virtue of its ability to form films at several surfaces, the high stability in redox processes as well as the reproducibility of preparations.

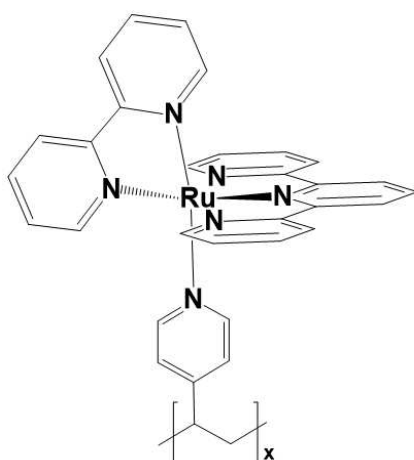


Figure 11: $[\text{Ru}(\text{tpy})(\text{bpy})(\text{VP})_x]^{2+}$ complex. Adapted from Calvert and Meyer.⁶⁸

Use of ruthenium(II) polypyridyl complexes for modifying electrode surfaces are interesting by virtue of the remarkable properties mentioned. In this work, we varied the heteroaryl-2-imidazole ligands in the four ruthenium(II) terpyridine complexes such that the HOMO and LUMO are modified. This in turn is expected to influence on properties of the complexes, specifically, to modulate the oxidation potential of the ruthenium(II) terpyridine complexes that will be used to modify the electrodes.

Given the interesting features exhibited by N-heterocycles compounds, we were interested in tuning the redox potentials and MLCT energies of ruthenium(II) terpyridine complexes containing heteroaryl-2-imidazole ligands taking advantage of their σ -donor/ π -acceptor properties. Ligands 2-(1H-imidazol-2-yl)pyridine (**Himpy**), 2-(1H-imidazol-2-yl)pyrazine (**Himpz**), 2-(1H-imidazol-2-yl)pyrimidine (**Himpm**) and 3-(1H-imidazol-2-yl)pyridazine (**Himpa**) were systematically chosen as they differ in σ -donor behavior because of different heteroaryl ring acidity which influences on basicity of imidazole ring, and this can directly influence on oxidation potentials of

ruthenium(II). Furthermore, reduction potentials are expected to be influenced by π -acceptor behavior of heteroaryl ring, and that can shift MLCT energies as they are also related to LUMO energies.

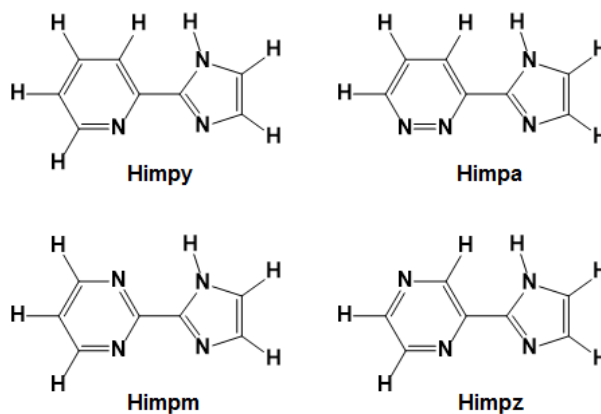


Figure 12: Heteroaryl-2-imidazole ligands.

[Ru(tpy)Cl₃] was chosen as the precursor complex because of its facile synthesis and good yield obtained. All ligands used for synthesis of Ru(II) complexes were purified before use. Complex structures are shown below.

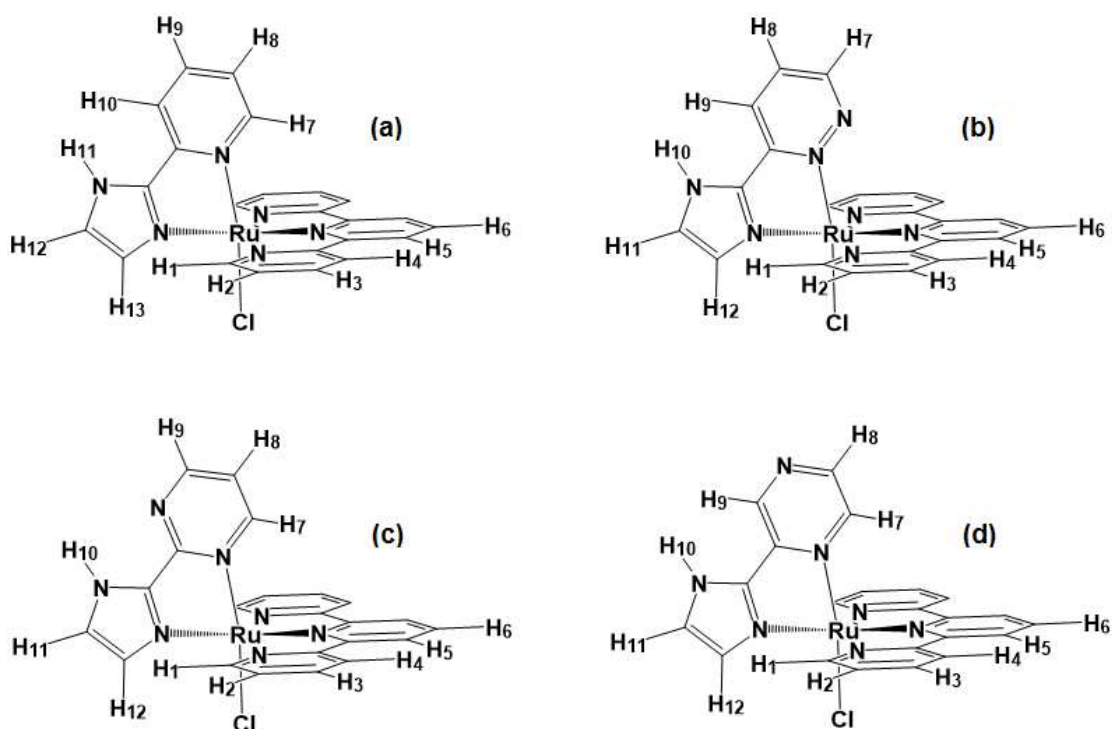


Figure 13: Ru(II) complexes structures. **(a)** [RuCl(Himpy)(tpy)]⁺, **(b)** [RuCl(Himpa)(tpy)]⁺, **(c)** [RuCl(Himpm)(tpy)]⁺ and **(d)** [RuCl(Himpz)(tpy)]⁺.

2. Aim

The project aims to modulate the electronic structure of four new ruthenium(II) complexes $[\text{RuCl}(\text{Himpa})(\text{tpy})]^+$, $[\text{RuCl}(\text{Himpm})(\text{tpy})]^+$, $[\text{RuCl}(\text{Himpy})(\text{tpy})]^+$, $[\text{RuCl}(\text{Himpz})(\text{tpy})]^+$ by changing the heteroaryl-2-imidazole ligands featuring different donor-acceptor electronic properties.

3. Experimental

3.1 Materials and measurements

Materials

Aminoacetaldehyde dimethyl acetal (98%, Sigma Aldrich), ammonium hexafluorophosphate (NH_4PF_6 , $\geq 95\%$, Sigma Aldrich), lithium chloride (99%, Merck), multi-walled carbon nanotubes (MWCNTs, 95%, CNT Co., Ltd.), external diameter: 10-40 nm, length: 5-20 μm , neutral aluminum oxide for chromatography (pH suspension 10% in H_2O 6.5-7.5, Carlo Erba Reagents), poly(4-vinylpyridine) (P4VP, 99%, Mw = 160.000, Aldrich), pyridazine-3-carbonitrile (99%, Aldrich), triethylamine (99%, Vetec-Sigma Brazil), ruthenium trichloride anhydrous ($\text{RuCl}_3 \cdot x\text{H}_2\text{O}$, Sigma Aldrich), 2,2':6',2''-terpyridine (tpy, 98%, Aldrich). Acetone, acetonitrile, chloroform, dichloromethane, diethyl ether, N,N-dimethylformamide, dimethylsulphoxide, absolute ethanol, ethyl acetate, glacial acetic acid, hydrochloric acid, methanol, and potassium carbonate were purchased from Labsynth. All the chemicals were used as received without further purification. Himpy, Himpm and Himpz ligands were synthesized according to literature⁶⁹ and obtained from the Formiga Research Group.

Measurements

Conductivity measurements of the four $[\text{RuCl}(\text{L})(\text{tpy})]\text{PF}_6$ solutions (L: Himpy, Himpa, Himpm, Himpz) were obtained using a Mca-150 conductimeter. Sonication was performed on a Thornton Inpec Eletrônica Ultrasound machine (Model 4L). Electrical conductivity of the films were obtained using a four-point probe (Cascade Microtech C4S-64) coupled to an electrometer (Keithley 617) and a digital multimeter (Minipa ET-2500). Electronic spectra in the 200-800 nm range were recorded on a Bel UV-M51 UV-vis spectrophotometer. ^1H and ^{13}C NMR spectra were recorded on Bruker Avance 400 and 500 MHz spectrometers. ^1H - ^1H Correlation Spectroscopy (COSY), ^1H - ^{13}C Heteronuclear Multiple Bond Correlation (HMBC) and Heteronuclear Single Quantum Correlation (HSQC) spectra were recorded on a Bruker Avance 400 MHz spectrometer. Electrospray ionization mass spectroscopy (ESI-MS) measurements were carried out on a Waters Quattro Micro API mass spectrometer. Elemental analysis were acquired on a Perkin Elmer 2400 CHN analyzer. X-ray diffraction measurements were made on a Bruker Kappa Apex II Duo diffractometer operating with Cu and Mo sources. Electrochemical measurements were performed on a Metrohm Autolab PGSTAT12 potentiostat, using a three-

electrode system consisting of a Pt working electrode, Ag/AgNO₃ as a reference electrode and Pt wire auxiliary electrode, as well as TBAPF₆ (0.1 mol L⁻¹ in acetonitrile) as the supporting electrolyte. The potentials were referred against ferrocene/ferrocenium couple (0.14 V vs. Ag/AgNO₃ reference). The concentrations of the Ru²⁺ complexes used for the measurements were 2x10⁻³ mol L⁻¹.

3.2 Preparation of films for conductivity measurements

The MWCNT/P4VP and MWCNT/P4VP-Fe(CN)₅ (metallopolymer) films were prepared as follows. MWCNT (25 mg) was added to the P4VP ethanolic solution (5 mL, 10 mg mL⁻¹) and the solution was sonicated (240 W) for 1 hour. After that, the solution was centrifuged at 4500 rpm for 10 minutes and the supernatant dispersion was separated to be used in the film preparation. In addition, MWCNT (25 mg) was added to metallopolymer solution (5 mL, 21.25 mg mL⁻¹) and the process was followed in the same way as described above in order to obtain the MWCNT-metallopolymer dispersion. These dispersions were then dropped onto the Teflon substrates, and dried by supplying a subtle flow of nitrogen at room temperature. This process was repeated until the films occupied the total volume (15 mm of diameter, 2.2 mm of thickness). Finally, the films were dried under vacuum at 40°C for 4 hours. The films could then be peeled off from the Teflon substrates to give samples with 2.2 mm of thickness.

3.3 Synthesis of [Ru(tpy)Cl₃]

The complex [Ru(tpy)Cl₃] was prepared according to the reported procedure.⁷⁰ To a 100 mL round-bottom flask containing 30 mL of boiling absolute ethanol was added 103.7 mg (0.5 mmol) of RuCl₃.xH₂O and refluxed under stirring for 5 minutes. After that, 2,2':6',2''-terpyridine (30 mL, 3.9 mg mL⁻¹, 0.5 mmol) was added dropwise. The mixture was heated under reflux for 3 hours under vigorous magnetic stirring. After this time, the reaction was left to cool to room temperature and left in a refrigerator overnight. The fine dark brown powder appearing was filtered from the brown solution. The product was washed with 3x15 mL portions of absolute ethanol followed by 3x15 mL portions of diethyl ether and air-dried until constant mass. Yield: 175 mg, 79%. Elemental analysis for [RuC₁₅H₁₁N₃Cl₃].H₂O, Calculated (%): C, 39.28; H, 2.85; N, 9.16. Found (%): C, 38.71; H, 2.81; N, 8.93. ESI-MS

(CH₃CN) *m/z*: 404.9 [M-Cl]⁺. UV-vis [λ_{max} , nm (ϵ , L mol⁻¹ cm⁻¹) in CH₃CN]: 227 (9951), 269 (4393), 280 (4228), 309 (4822), 317 (4741), 335 (sh), 404 (1458), 462 (679).

3.4 Synthesis of 3-(1H-imidazol-2-yl)pyridazine – Himpa

The ligand was prepared according to the reported procedure.⁶⁹ To a 25-mL round-bottom flask containing 105.1 mg (1 mmol) of 3-pyridazine-carbonitrile and 400 μ L of methanol, 18.8 μ L (0.1 mmol) of a 30% solution of sodium methoxide in methanol was added. The reaction mixture was stirred for 1 hour at room temperature. 109 μ L (1 mmol) of aminoacetaldehyde dimethyl acetal followed by dropwise addition of 110 μ L (2 mmol) of glacial acetic acid were added to the reaction mixture and then heated under reflux for 30 minutes. After cooling to room temperature, 600 μ L of methanol and 500 μ L of HCl 6 mol L⁻¹ were added, and the mixture was heated under reflux for 5 hours. After that, the solution was evaporated to dryness and a freshly prepared warm solution of K₂CO₃ (1 g mL⁻¹) was added carefully, bringing pH to 10. The resulting suspension was left in a refrigerator for 12 hours. After that, the solid appearing was filtered from the solution and washed with 3x5 mL portions of diethyl ether. Ultimately, the product was extracted with chloroform, and after leaving the solvent to evaporate slowly, pale red crystals were obtained. Yield: 89.1 mg, 61%. Elemental analysis for [3(C₇H₆N₄).H₂O], Calculated (%): C, 55.25; H, 4.42; N, 36.82. Found (%): C, 55.85; H, 4.41; N, 36.87. ESI-MS (CH₃OH) *m/z*: 147.0 [M+H]⁺. ¹H-NMR (500 MHz, DMSO-d₆): δ 13.34 (s, 1H), 9.20 (dd, 1H, *J* = 5.0, 1.5 Hz), 8.24 (dd, 1H, *J* = 8.5, 1.5 Hz), 7.79 (dd, 1H, *J* = 8.5, 5.0 Hz), 7.32 (s, 1H), 7.23 (s, 1H). ¹³C-NMR (125.7 MHz, DMSO-d₆): δ 152.1, 151.4, 143.5, 130.6, 128.3, 123.6, 120.3. UV-vis [λ_{max} , nm (ϵ , L mol⁻¹ cm⁻¹) in CH₃OH]: 284 (10787).

3.5 Synthesis of [RuCl(Himpy)(tpy)]Cl

The complex was prepared following the reported procedure.⁷¹ [Ru(tpy)Cl₃] (44.0 mg, 0.1 mmol) was added to a 50-mL round-bottom flask containing 25 mL of absolute ethanol and then refluxed under stirring for 30 minutes. After that, triethylamine (30 μ L, 0.2 mmol) and then Himpy (14.5 mg, 0.1 mmol) were added to the reaction mixture and the reflux condition was continued for 6 hours. After cooling to room temperature, the volume of the filtrate was reduced to 5 mL and this suspension was left in a refrigerator overnight. The dark violet solid was collected by vacuum filtration, washed with cold water and ether, and dried on a desiccator.

The product was chromatographed on neutral alumina column by increasing polarity of the eluting mixture of solvents, being them CH₃CN:CH₂Cl₂, from 1:100 to 1:2 (v/v), and then C₂H₅OH:CH₂Cl₂ 1:10 (v/v). A violet fraction was collected and the solvent removed under reduced pressure. Yield: 8.24 mg, 15%. Elemental analysis for [RuC₂₃H₁₈N₆Cl]Cl, Calculated (%): C, 50.19; H, 3.29; N, 15.27. Found (%): C, 51.17; H, 3.21; N, 15.27. ESI-MS (CH₃CN) m/z: 515.4 [M-Cl]⁺. ¹H-NMR (400 MHz, DMSO-d₆): δ 8.77 (d, 2H, *J* = 8.0 Hz), 8.66 (d, 2H, *J* = 8.0 Hz), 8.31 (d, 1H, *J* = 7.8 Hz), 8.12 (d, 1H, *J* = 1.0 Hz), 8.11 (t, 1H, *J* = 8.0 Hz), 8.03 (d, 1H, *J* = 1.0 Hz), 7.96 (td, 2H, *J* = 7.8, 1.4 Hz), 7.73 (d, 2H, *J* = 5.5 Hz), 7.72 (td, 1H, *J* = 7.8, 1.2 Hz), 7.43 (ddd, 2H, *J* = 7.8, 5.5, 1.2 Hz), 7.02 (d, 1H, *J* = 5.5 Hz), 6.90 (ddd, 1H, *J* = 7.8, 5.5, 1.2 Hz).

3.6 Synthesis of [RuCl(Himpy)(tpy)]PF₆

The complex was prepared following the reported procedure.⁷¹ [Ru(tpy)Cl₃] (44.0 mg, 0.1 mmol) was added to a 50-mL round-bottom flask containing 25 mL of absolute ethanol and then refluxed under stirring for 30 minutes. After that, triethylamine (30 μL, 0.2 mmol) and then Himpy (21.8 mg, 0.15 mmol) were added to the reaction mixture and the reflux condition was continued for 3 hours. Lithium chloride in ethanol (2 mL, 10 mg mL⁻¹) was then added, and after one extra hour under reflux, the mixture was filtered while hot. After cooling to room temperature, the volume of the filtrate was reduced to 2 mL and added to an aqueous solution of NH₄PF₆ (5 mL, 10 mg mL⁻¹). The suspension was left in a refrigerator overnight, and the formed product was collected by vacuum filtration and washed with cold water, chloroform and ether, and dried on a desiccator. Yield: 39.5 mg, 60%. Elemental analysis for [RuC₂₃H₁₈N₆Cl]PF₆, Calculated (%): C, 41.86; H, 2.75; N, 12.73. Found (%): C, 41.96; H, 2.70; N, 12.90. ESI-MS (CH₃CN) m/z: 515.0 [M-PF₆]⁺. ¹H-NMR (400 MHz, DMSO-d₆): δ 8.77 (d, 2H, *J* = 8.0 Hz), 8.66 (d, 2H, *J* = 8.0 Hz), 8.16 (d, 1H, *J* = 1.0 Hz), 8.12 (t, 1H, *J* = 8.0 Hz), 8.11 (d, 1H, *J* = 8.0 Hz), 8.05 (d, 1H, *J* = 1.0 Hz), 7.97 (td, 2H, *J* = 8.0, 1.0 Hz), 7.73 (d, 2H, *J* = 6.0 Hz), 7.72 (m, 1H, *J* = 1.0 Hz), 7.43 (ddd, 2H, *J* = 8.0, 6.0, 1.0 Hz), 7.05 (d, 1H, *J* = 5.5 Hz), 6.90 (ddd, 1H, *J* = 8.0, 5.5, 1.0 Hz). UV-vis [λ_{\max} , nm (ϵ , L mol⁻¹ cm⁻¹) in CH₃CN]: 237 (19324), 278 (16165), 318 (22541), 413 (sh), 518 (4324).

3.7 Synthesis of [RuCl(Himpa)(tpy)]PF₆

The complex was prepared following the same procedure for [RuCl(Himpy)(tpy)]PF₆ using [Ru(tpy)Cl₃] (44.0 mg, 0.1 mmol), triethylamine (30 μ L, 0.2 mmol), Himpa (21.9 mg, 0.15 mmol), lithium chloride (2 mL, 10 mg mL⁻¹), NH₄PF₆ (5 mL, 10 mg mL⁻¹). Yield: 47.5 mg, 72%. Elemental analysis for [RuC₂₂H₁₇N₇Cl]PF₆.2H₂O, Calculated (%): C, 37.91; H, 3.04; N, 14.07. Found (%): C, 37.30; H, 2.77; N, 13.59. ESI-MS (CH₃CN) m/z: 516.0 [M-PF₆]⁺. ¹H-NMR (400 MHz, DMSO-d₆): δ 8.62 (d, 2H, *J* = 8.0 Hz), 8.55 (d, 2H, *J* = 8.0 Hz), 8.07 (dd, 1H, *J* = 4.8, 2.0 Hz), 7.97 (t, 1H, *J* = 8.0 Hz), 7.90 (td, 2H, *J* = 8.0, 1.6 Hz), 7.85 (s, 1H), 7.79 (dd, 1H, *J* = 8.4, 2.0 Hz), 7.69 (d, 2H, *J* = 4.8 Hz), 7.61 (s, 1H), 7.41 (ddd, 2H, *J* = 8.0, 4.8, 1.6 Hz), 7.14 (dd, 1H, *J* = 8.4, 4.8 Hz). UV-vis [λ_{max} , nm (ϵ , L mol⁻¹ cm⁻¹) in CH₃CN]: 237 (46563), 276 (43890), 313 (57293), 364 (6316), 441 (13616), 496 (15956).

3.8 Synthesis of [RuCl(Himpm)(tpy)]PF₆

The complex was prepared following the same procedure for [RuCl(Himpy)(tpy)]PF₆ using [Ru(tpy)Cl₃] (44.0 mg, 0.1 mmol), triethylamine (30 μ L, 0.2 mmol), Himpm (21.9 mg, 0.15 mmol), lithium chloride (2 mL, 10 mg mL⁻¹), NH₄PF₆ (5 mL, 10 mg mL⁻¹). Yield: 42.2 mg, 64%. Elemental analysis for [RuC₂₂H₁₇N₇Cl]PF₆, Calculated (%): C, 39.98; H, 2.59; N, 14.84. Found (%): C, 39.58; H, 2.23; N, 13.76. ESI-MS (CH₃CN) m/z: 516.0 [M-PF₆]⁺. ¹H-NMR (500 MHz, DMSO-d₆): δ 8.72 (d, 2H, *J* = 8.0 Hz), 8.63 (d, 2H, *J* = 8.0 Hz), 8.31 (dd, 1H, *J* = 5.0, 2.0 Hz), 8.02 (t, 1H, *J* = 8.0 Hz), 7.93 (td, 2H, *J* = 8.0, 1.0 Hz), 7.92 (s, 1H), 7.70 (d, 1H, *J* = 5.0 Hz), 7.68 (s, 1H), 7.46 (ddd, 2H, *J* = 8.0, 5.0, 1.0 Hz), 6.97 (dd, 1H, *J* = 5.0, 2.0 Hz), 6.53 (t, 1H, *J* = 5.0 Hz). UV-vis [λ_{max} , nm (ϵ , L mol⁻¹ cm⁻¹) in CH₃CN]: 237 (47531), 276 (49210), 307 (sh), 315 (52390), 383 (10386), 426 (11198), 502 (12692).

3.9 Synthesis of [RuCl(Himpz)(tpy)]PF₆

The complex was prepared following the same procedure for [RuCl(Himpy)(tpy)]PF₆ using [Ru(tpy)Cl₃] (44.0 mg, 0.1 mmol), triethylamine (30 μ L, 0.2 mmol), Himpz (21.9 mg, 0.15 mmol), lithium chloride (2 mL, 10 mg mL⁻¹), NH₄PF₆ (5 mL, 10 mg mL⁻¹). Yield: 51.4 mg, 78%. Elemental analysis for [RuC₂₂H₁₇N₇Cl]PF₆.2H₂O, Calculated (%): C, 37.91; H, 3.04; N, 14.07. Found (%): C, 38.35; H, 2.40; N, 13.77. ESI-MS (CH₃CN) m/z: 516.0 [M-PF₆]⁺. ¹H-NMR (500 MHz,

DMSO- d_6): δ 8.76 (d, 1H, $J = 1.0$ Hz), 8.74 (d, 2H, $J = 8.0$ Hz), 8.63 (d, 2H, $J = 8.0$ Hz), 8.06 (t, 1H, $J = 8.0$ Hz), 7.95 (td, 2H, $J = 8.0, 1.0$ Hz), 7.84 (s, 1H), 7.64 (s, 1H), 7.63 (d, 2H, $J = 5.5$ Hz), 7.54 (d, 1H, $J = 3.5$ Hz), 7.45 (ddd, 2H, $J = 8.0, 5.5, 1.0$ Hz), 6.81 (dd, 1H, $J = 3.5, 1.0$ Hz). UV-vis [λ_{\max} , nm (ϵ , L mol $^{-1}$ cm $^{-1}$) in CH $_3$ CN]: 237 (23834), 278 (17632), 318 (25667), 368 (8684), 440 (5094), 522 (6598).

4. Results and discussions

4.1 [Ru(tpy)Cl₃] complex

The precursor complex was synthesized by using stoichiometric molar quantities of RuCl₃ and terpyridine in a simple reaction under reflux.

The complex is soluble in DMSO and DMF, slightly soluble in CH₃CN and practically insoluble in water, methanol, ethanol, acetone, ethyl acetate, chloroform, dichloromethane and diethyl ether, all of them at room temperature. Although many research articles are available related to synthesis of terpyridine-derivatives Ru(III) complexes,^{70,72–75} the way it is carried out is not well detailed. Just simple mixing between RuCl₃ and terpyridine solutions and subsequent reaction under reflux gave a brown solid. On the other hand, dropwise addition of terpyridine solution to ruthenium chloride solution and posterior refluxing condition gave a fine dark brown powder. Due to the paramagnetic nature of the Ru(III), acquirement of ¹H-NMR spectrum of the complex [Ru(tpy)Cl₃] was not useful as broad bands lacking of information were obtained, but adding powdered Zn to a solution of that complex yielded a diamagnetic sample,⁷⁶ thus allowing to obtain useful spectra to differentiate them. According to both spectra, simple mixing of ruthenium chloride and ligand solutions leads to an impure compound (**Figure 14**), while dropwise addition of terpyridine to ruthenium solution gives a probable pure compound (**Figure 15a**). Those impurities could be related to formation of [Ru(tpy)₂]²⁺, and this situation seems to be avoided at adding dropwise terpyridine as ruthenium is in excess quantity. Those spectra are not related exactly to the precursor complex with three chloride ligands, as DMSO solvent can substitute one of them.⁷⁶ But despite of precursor purity, the final [RuCl(L)(tpy)]⁺ complexes synthesized using both pure and impure precursor complex were obtained without significant differences.

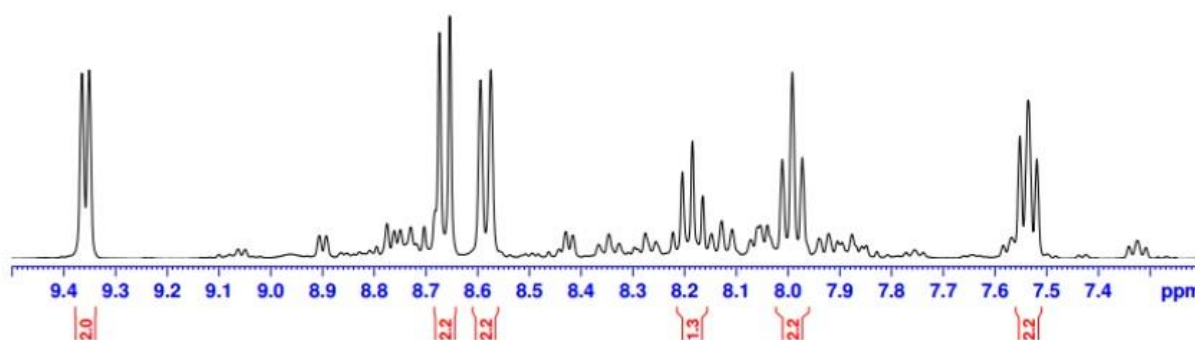


Figure 14: ¹H-NMR spectra of impure precursor complex after reduction with Zn in DMSO-d₆.

Figure 15 shows $^1\text{H-NMR}$ of both complex after reduction with powdered Zn and free terpyridine ligand. Peak assignments were made through use of characteristic proton-proton coupling constants for heterocyclic aromatic compounds⁷⁷ along with integration obtained from spectra and are shown in **Table 1**. As expected, H₁ is largely deshielded after coordination because adjacent nitrogen releases electronic density over the ruthenium center which reduces its electron density. H₅ and H₆ are also deshielded, whereas H₃ and H₄ experience an upfield shift, showing that inductive effects and π backbonding⁷⁸ are variable in each pyridine moiety.

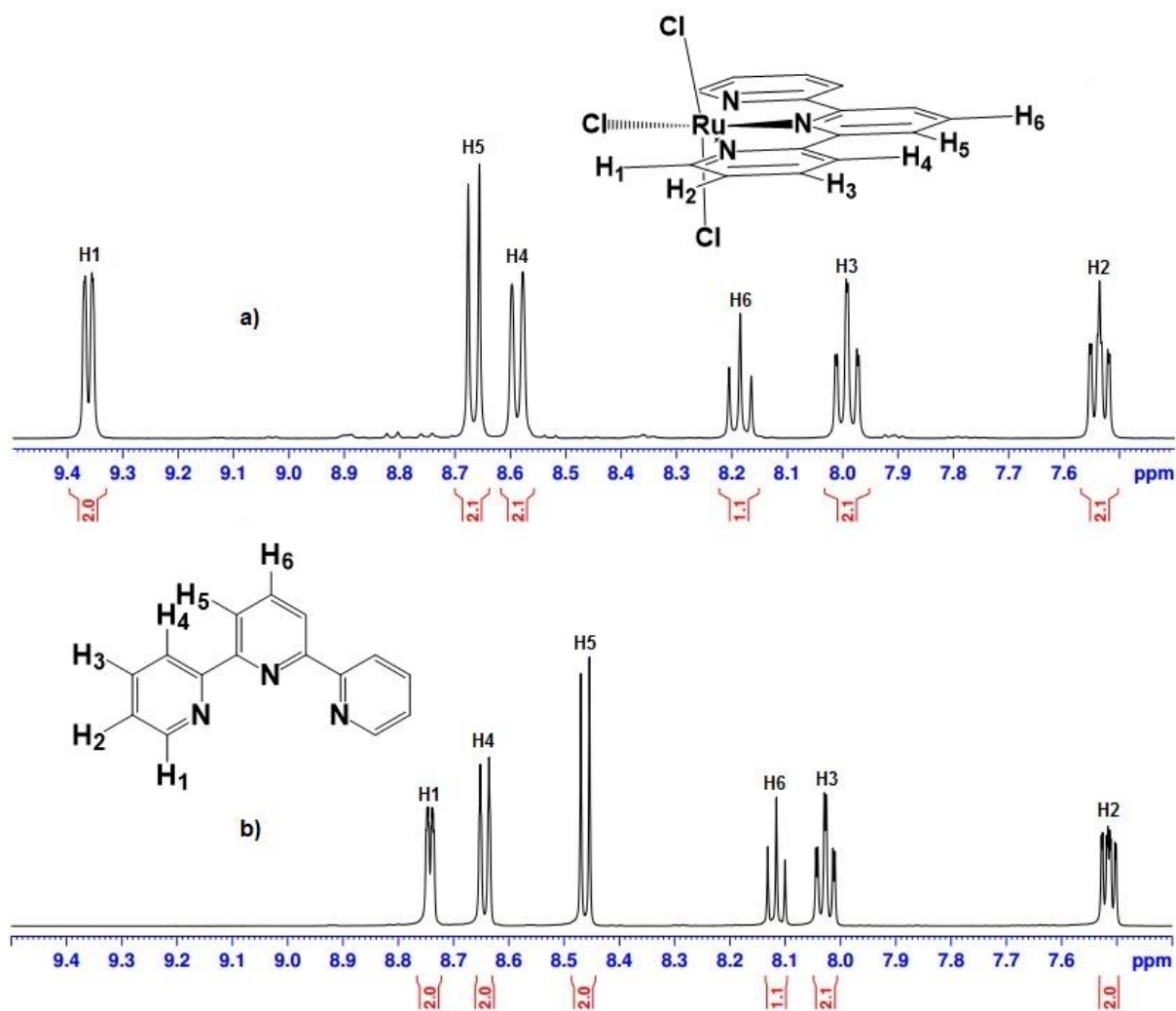


Figure 15: $^1\text{H-NMR}$ spectra of both (a) $[\text{Ru}(\text{tpy})\text{Cl}_3]$ reduced with Zn and (b) terpyridine in DMSO-d_6 .

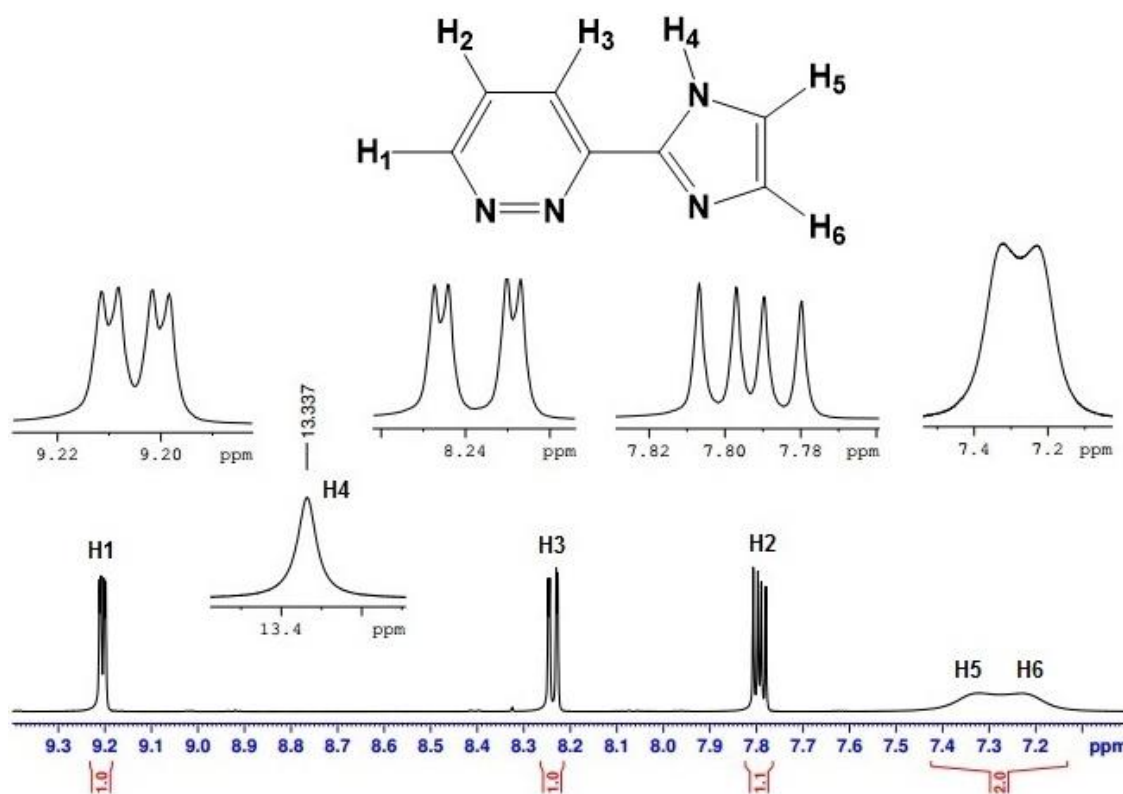
Table 1: $^1\text{H-NMR}$ data for terpyridine (**1**) and $[\text{Ru}(\text{tpy})\text{Cl}_3]$ reduced with Zn (**2**).

Hydrogen	δ (ppm)		J (Hz)
	(1)	(2)	
H1	8.74	9.36	5.6, 1.2
H2	8.64	8.58	7.8, 5.6, 1.2
H3	8.46	8.66	7.8, 1.2
H4	8.12	8.18	7.8
H5	8.03	7.99	8.0
H6	7.51	7.53	8.0

In order to make the study with heteroaryl-2-imidazole ligands, the 3-(1H-imidazol-2-yl)pyridazine "Himpa" ligand was synthesized.

4.2 3-(1H-imidazol-2-yl)pyridazine "Himpa"

The $^1\text{H-NMR}$ spectrum of 3-(1H-imidazol-2-yl)pyridazine "Himpa" is shown in **Figure 16**. Five resonance peaks are observed, one of them being two peaks slightly overlapped. The peak assignments are shown in **Table 2**. Pyridazine hydrogens H₁, H₂, and H₃ appear as doublets of doublets, while imidazole hydrogens H₄, H₅, and H₆ appear as broadened peaks.

**Figure 16:** $^1\text{H-NMR}$ spectrum of 3-(1H-imidazol-2-yl)pyridazine "Himpa" in DMSO- d_6 .

The hydrogen H₄, which is attached to the nitrogen of the imidazole ring, appears as a broad singlet due to the quadrupole moment of the nitrogen and rapid intermolecular proton exchange with H₂O (residual water), which leads to broadening of H₅ and H₆ because they become almost indistinguishable in the NMR time scale.

Table 2: ¹H-NMR data for 3-(1H-imidazol-2-yl)pyridazine “Himpa” recorded in DMSO-d₆.

Hydrogen	δ (ppm)	Signal	J (Hz)
H ₄	13.34	s	-
H ₁	9.20	dd	5, 1.5
H ₃	8.24	dd	8.5, 1.5
H ₂	7.79	dd	8.5, 5
H ₅	7.32	s	-
H ₆	7.23	s	-

The ¹³C-NMR spectrum of 3-(1H-imidazol-2-yl)pyridazine “Himpa” is shown in **Figure 17**. Seven resonance peaks are observed, as expected according to the proposed structure.

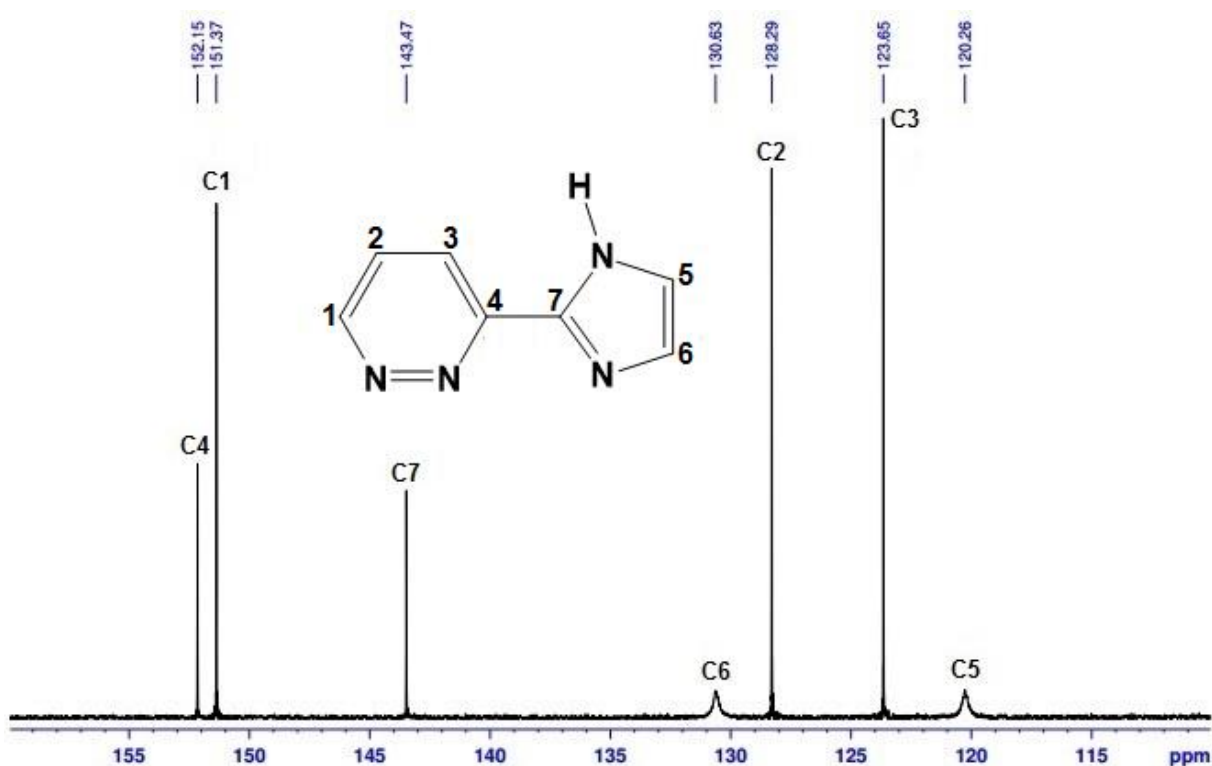


Figure 17: The ¹³C-NMR spectrum of 3-(1H-imidazol-2-yl)pyridazine “Himpa” in DMSO-d₆.

The peak assignments were possible through the combined use of 2D ^1H - ^{13}C HSQC and HMBC correlation spectroscopy, and are shown in **Table 3**. C₃, C₄ and C₂ are the most deshielded carbon atoms, as expected because they are adjacent to more electronegative nitrogen atoms, with C₃ and C₄ experiencing more downfield as they are in the electron-deficient pyridazine ring. It is also observed the broadening of C₁ and C₅, which is due to they are attached to the NMR time scale almost indistinguishable H₅ and H₆.

Table 3: ^{13}C -NMR data for 3-(1H-imidazol-2-yl)pyridazine “Himpa” recorded in DMSO- d_6 .

Carbon	δ (ppm)
C4	152.15
C1	151.37
C7	143.47
C6	130.63
C2	128.29
C3	123.65
C5	120.26

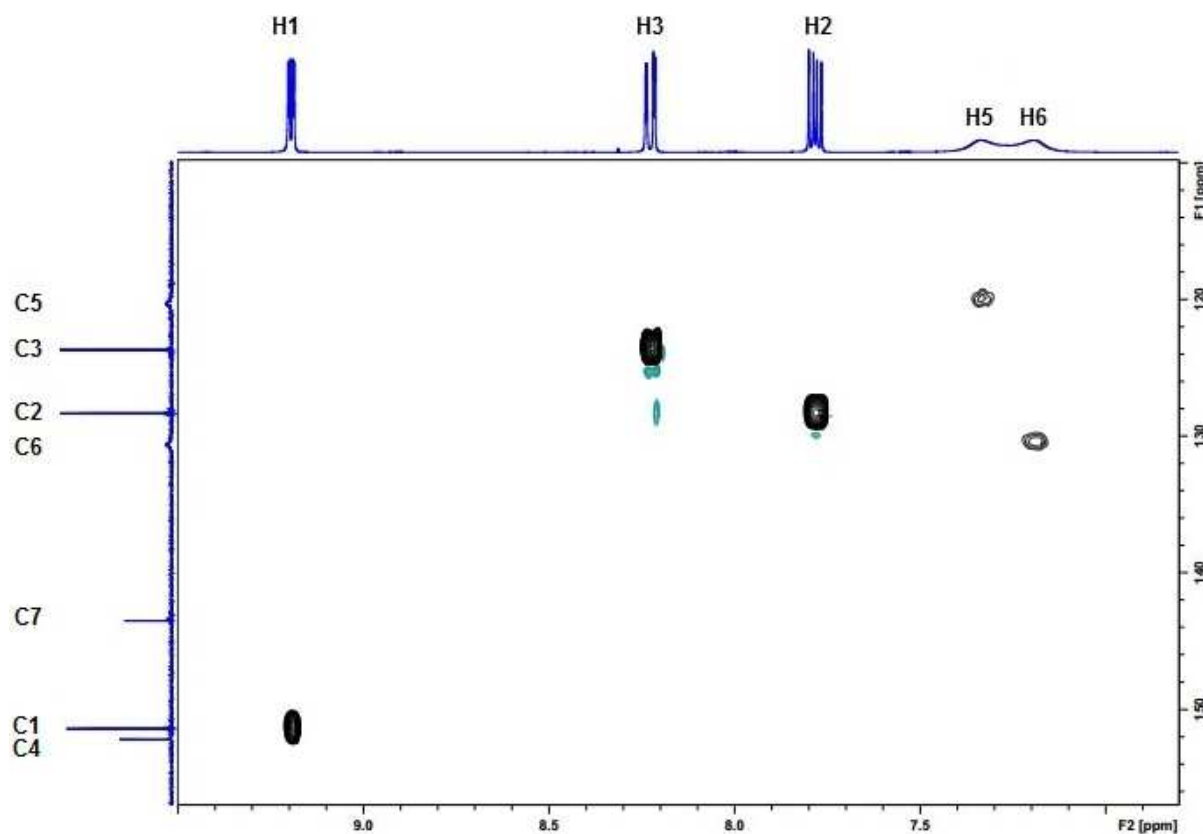


Figure 18: ^1H - ^{13}C HSQC spectrum of “Himpa” in DMSO- d_6 .

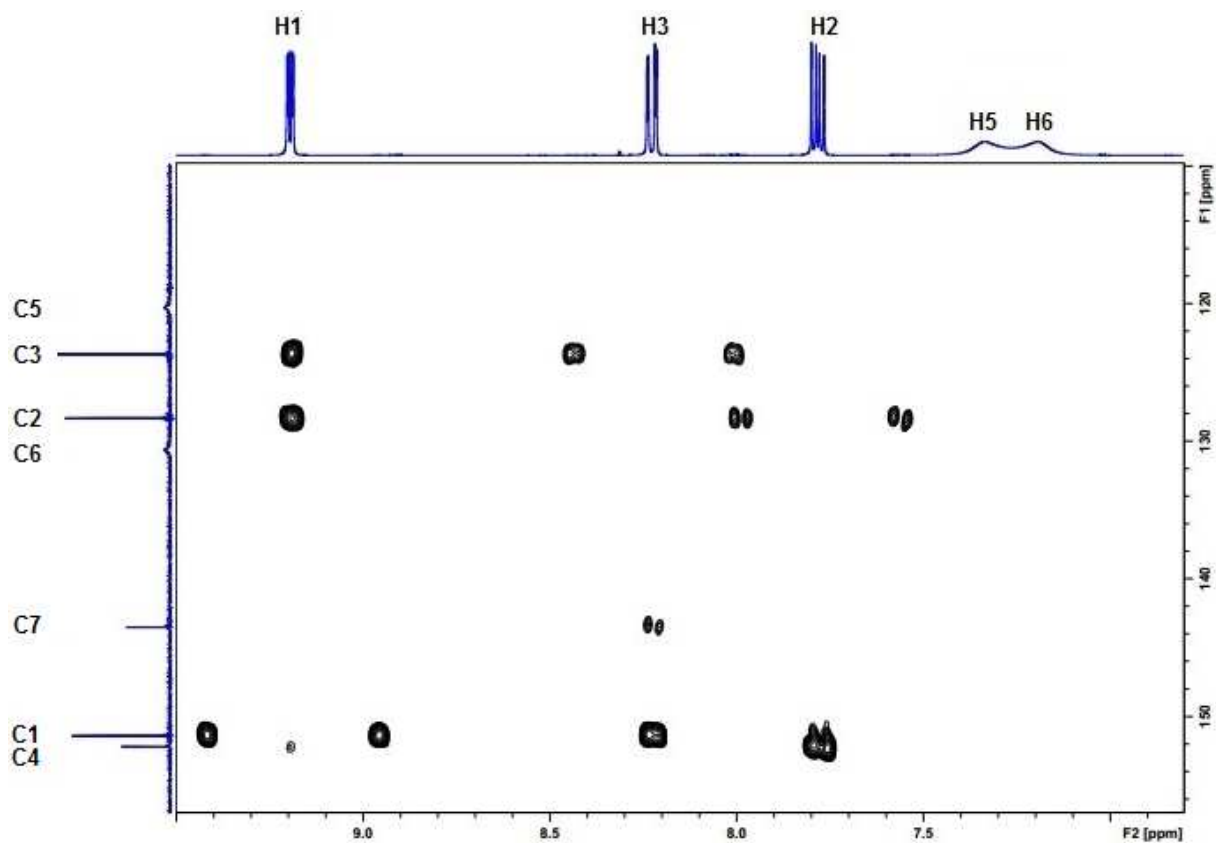


Figure 19: ^1H - ^{13}C HMBC spectrum of “Himpa” in DMSO-d_6 .

The structure was confirmed by X-ray crystallography. The ORTEP view of the molecular geometry is shown in **Figure 20**.

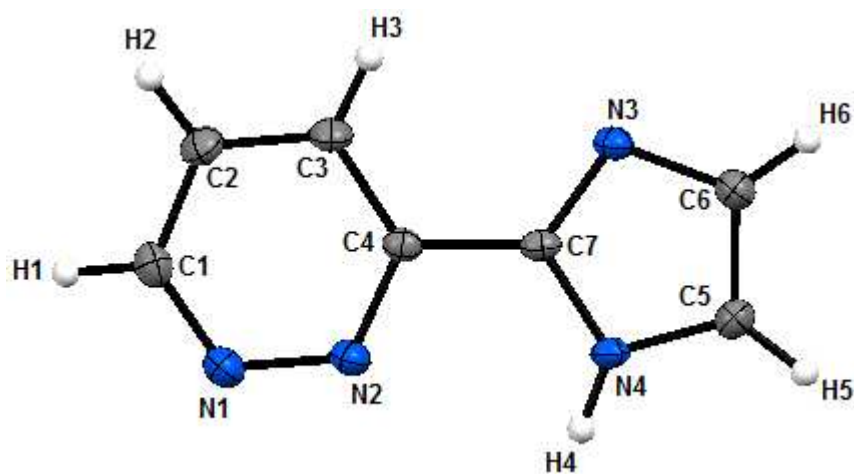


Figure 20: ORTEP view of the molecular geometry of 3-(1H-imidazol-2-yl)pyridazine “Himpa”.

The ligand is largely planar, since the dihedral angle between imidazole and pyridazine planes is 7.76°. The bond angles within pyridazine ring ranges from 117.16° to 123.64°, which are in close agreement with values for pyridazine ring (116.93°-123.91°).⁷⁹ The bond lengths between carbon and nitrogen atoms are lower (1.326-1.337 Å) than those between carbon atoms (1.370-1.398 Å). Furthermore, the bond angles and lengths of imidazole moiety is also in agreement with those reported for free imidazole ring⁸⁰. Crystallographic data for Himpa ligand are listed in **Table 4**. The bond angles and lengths for Himpa, free pyridazine and imidazole ligands are given in **Table 5**.

Table 4: Crystallographic data for 3-(1H-imidazol-2-yl)pyridazine “Himpa”.

Parameter	Himpa
Empirical formula	C ₇ H ₆ N ₄
Fw	146.15
Crystal symmetry	Orthorhombic
Space group	P b c a
a (Å)	10.915(2)
b (Å)	10.199(2)
c (Å)	12.829(3)
α, β, γ (°)	90.00
V (Å ³)	1428.5
Z	8
T (K)	273(2)

Table 5: Bond lengths (Å) and angles (°).

Atoms	Pyridazine	Imidazole	Himpa
N(2)-N(1)	1.345		1.344
N(1)-C(1)	1.325		1.326
C(1)-C(2)	1.395		1.390
C(2)-C(3)	1.371		1.370
C(1)-H(1)	0.978		0.930
C(2)-H(2)	0.933		0.930
N(4)-C(7)		1.349	1.357
C(7)-N(3)		1.326	1.328
N(3)-C(6)		1.378	1.375
C(6)-C(5)		1.358	1.366
N(2)-N(1)-C(1)	118.90		119.26
N(2)-C(1)-C(2)	123.91		123.64
C(1)-C(2)-C(3)	117.12		117.46
N(4)-C(7)-N(3)		111.3	111.41
C(7)-N(3)-C(6)		105.4	104.92
N(3)-C(6)-C(5)		109.8	110.48

4.3 Synthesis and characterization of [RuCl(L)(tpy)]⁺ complexes

Himpy, Himpm and Himpz were synthesized according to literature⁶⁹ and available in the laboratory. All the reactions for the synthesis of Ru(II) compounds were performed using triethylamine for reduction of Ru(III) to Ru(II) and excess of LiCl in order to avoid chloride labilization in the final products. Hexafluorophosphate counter-ion was chosen because of lower yields obtained with chloride counter-ion, as well as to take advantage of hexafluorophosphate salts being soluble in common solvents other than water compared to chloride salts. The compounds are soluble in DMSO, DMF, CH₃CN, H₂O, CH₃OH, C₂H₅OH and CH₃COCH₃, whereas are slightly soluble in CHCl₃ and CH₂Cl₂.

Molar conductivity values for the Ru(II) compounds in DMSO, CH₃CN, CH₃OH and C₂H₅OH indicate a complex:counterion 1:1 composition, whereas in water is not clear since the values are within the range for 1:1 and 1:2 electrolytes^{81,82} (**Table 6**). Such a behavior in water is likely due to the chloride labilization, which can be substituted by a water molecule resulting in the complex [Ru(H₂O)(L)(tpy)]²⁺.

Table 6: Molar conductivity of [RuCl(L)(tpy)]PF₆ compounds in different solvents at 25°C.

Compound	Acetonitrile	DMSO	Ethanol	Methanol	H ₂ O
[RuCl(Himpy)(tpy)]PF ₆	135.3	24.0	26.6	89.6	172.1
[RuCl(Himpa)(tpy)]PF ₆	152.2	38.4	25.9	100.0	159.4
[RuCl(Himpm)(tpy)]PF ₆	138.3	46.0	23.2	74.2	162.5
[RuCl(Himpz)(tpy)]PF ₆	122.1	25.7	26.7	81.8	163.9
Dissertation (1:1)	57-204	20-62	-	62-123	87-168
(2:1)	162-345	54-110	-	87-204	150-310
Geary, 1971 (1:1)	100-160	50-70	35-45	80-115	-
(2:1)	220-300	-	70-90	162-220	-

4.4 Mass spectrometry

The mass spectra of the complexes show an intense peak at m/z 515.0 or 516.0, related to [RuCl(L)(tpy)]⁺ with the isotopic pattern for ruthenium, thus confirming the presence of the molecular ion.

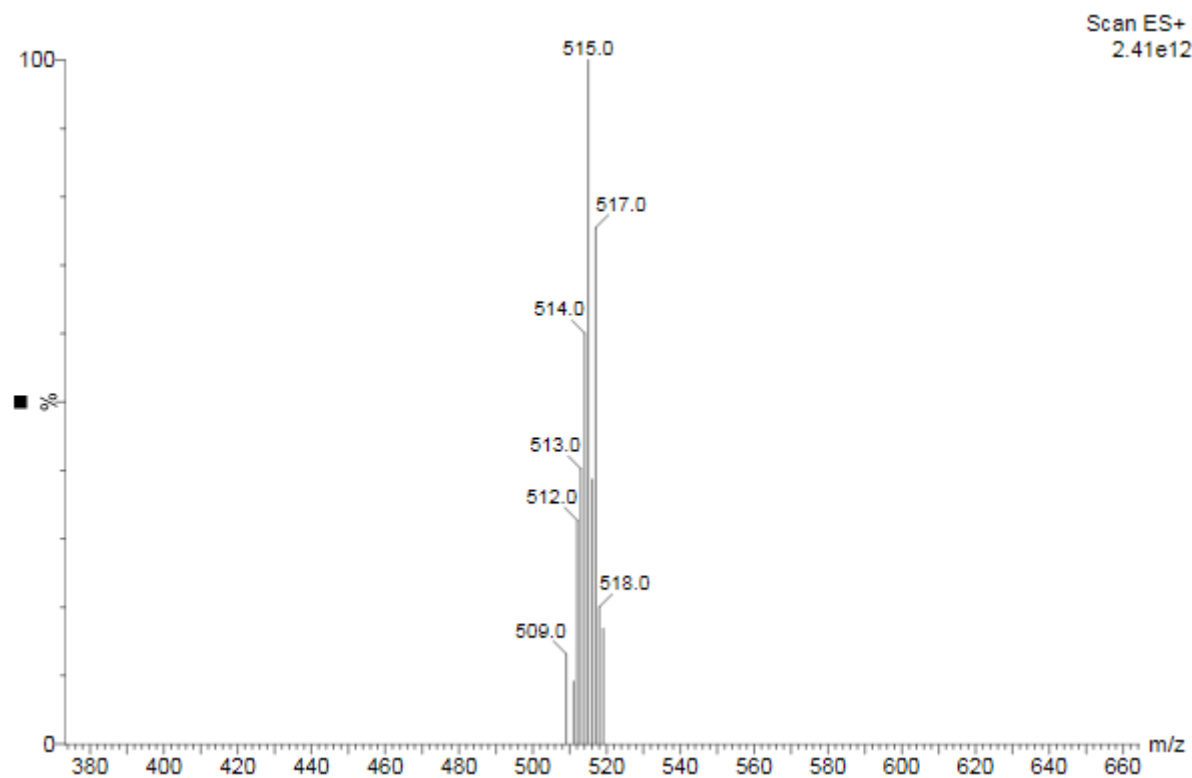


Figure 21: ESI-MS of the $[\text{RuCl}(\text{Himpy})(\text{tpy})]\text{PF}_6$ in acetonitrile.

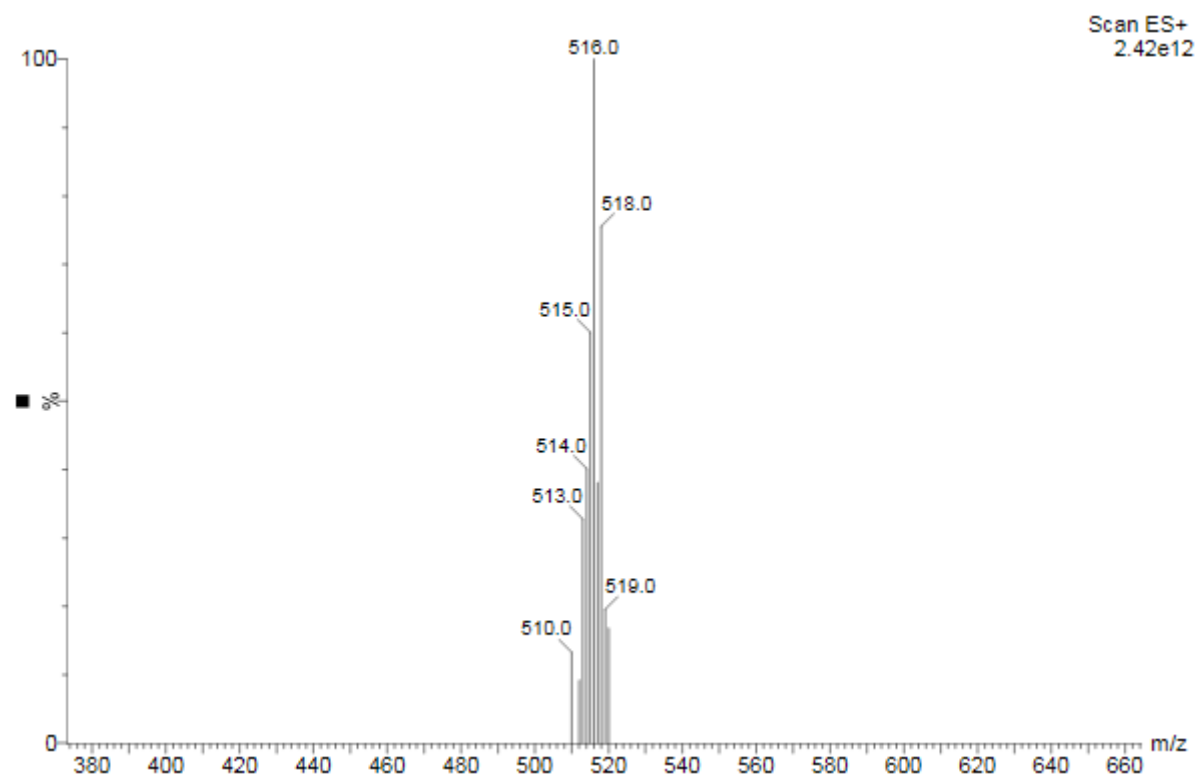


Figure 22: ESI-MS of the $[\text{RuCl}(\text{Himpa})(\text{tpy})]\text{PF}_6$ in acetonitrile.

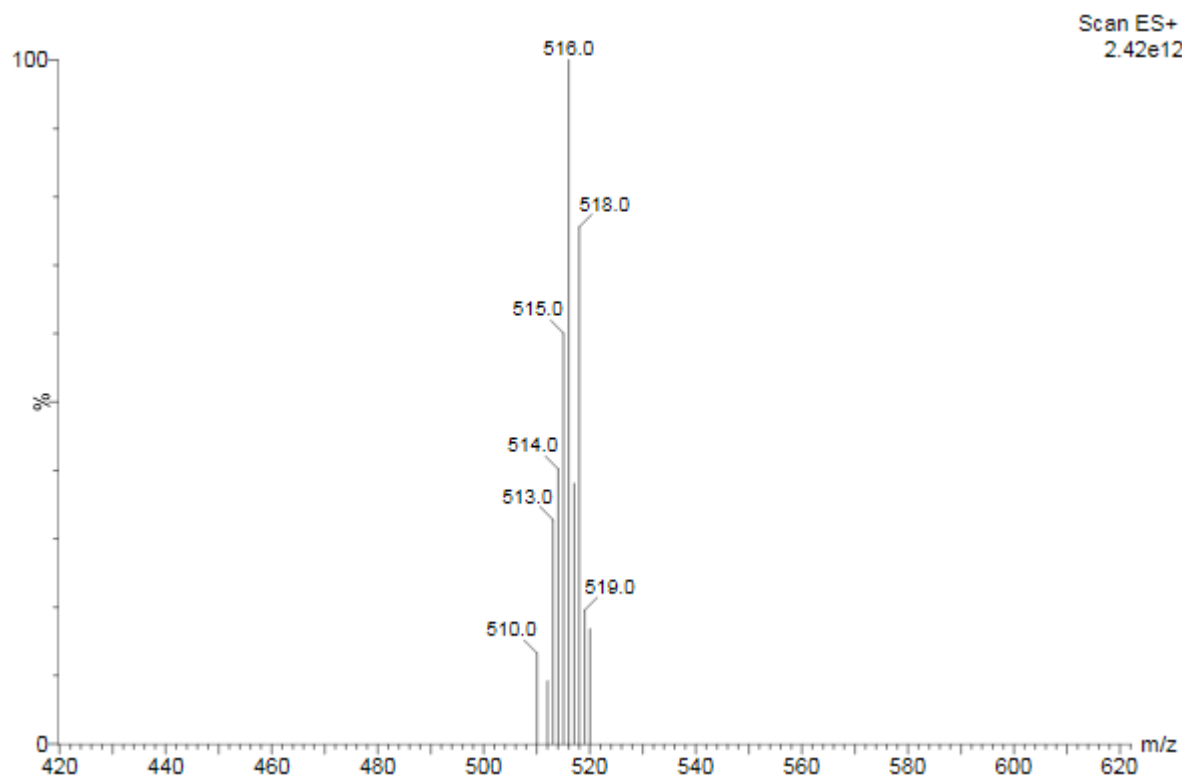


Figure 23: ESI-MS of the $[\text{RuCl}(\text{Himpm})(\text{tpy})]\text{PF}_6$ in acetonitrile.

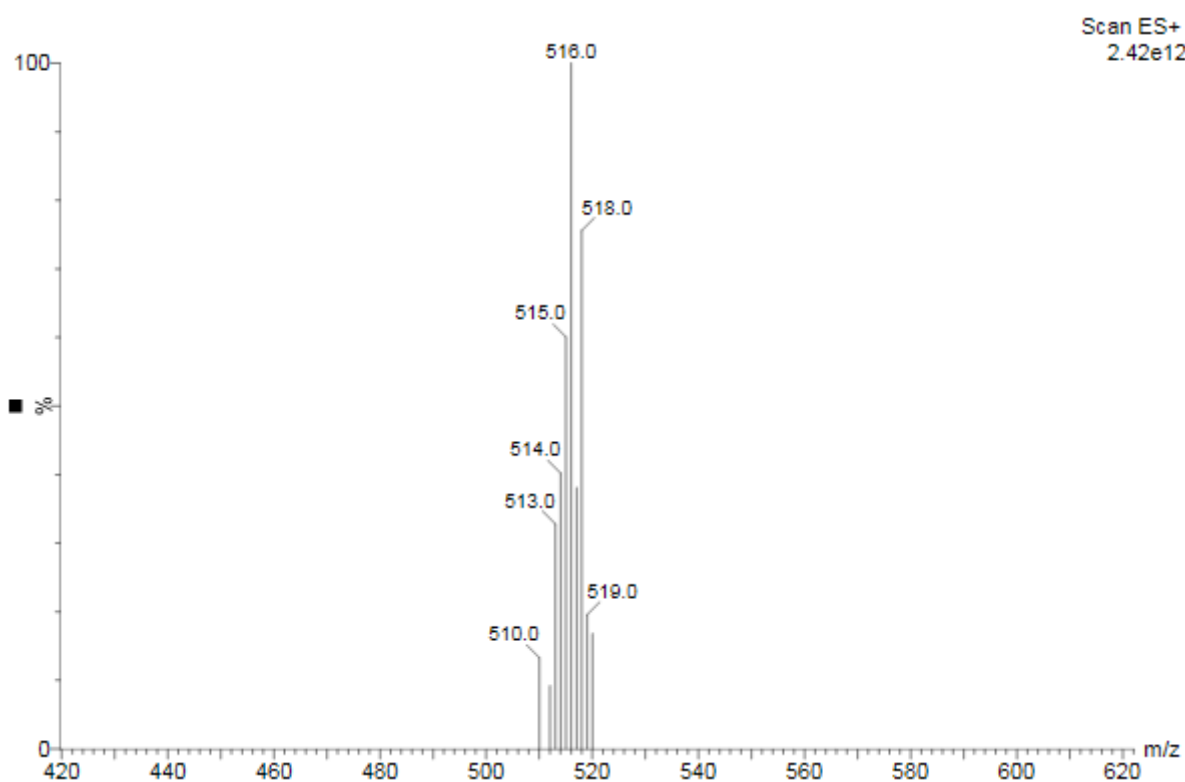


Figure 24: ESI-MS of the $[\text{RuCl}(\text{Himpz})(\text{tpy})]\text{PF}_6$ in acetonitrile.

4.5 $^1\text{H-NMR}$ spectroscopy of Ru(II) complexes and their crystal structures

The $^1\text{H-NMR}$ spectrum of the $[\text{RuCl}(\text{Himpy})(\text{tpy})]\text{Cl}$ compound was acquired in deuterated DMSO-d_6 solvent and is shown in **Figure 25**. According to the structure, 18 hydrogens are expected, but looking at the spectrum, one is missing. Assignments were made using the 2D ^1H COSY spectrum and crystal structure of the compound along with characteristic proton-proton coupling constants of heterocyclic aromatic compounds.⁷⁷

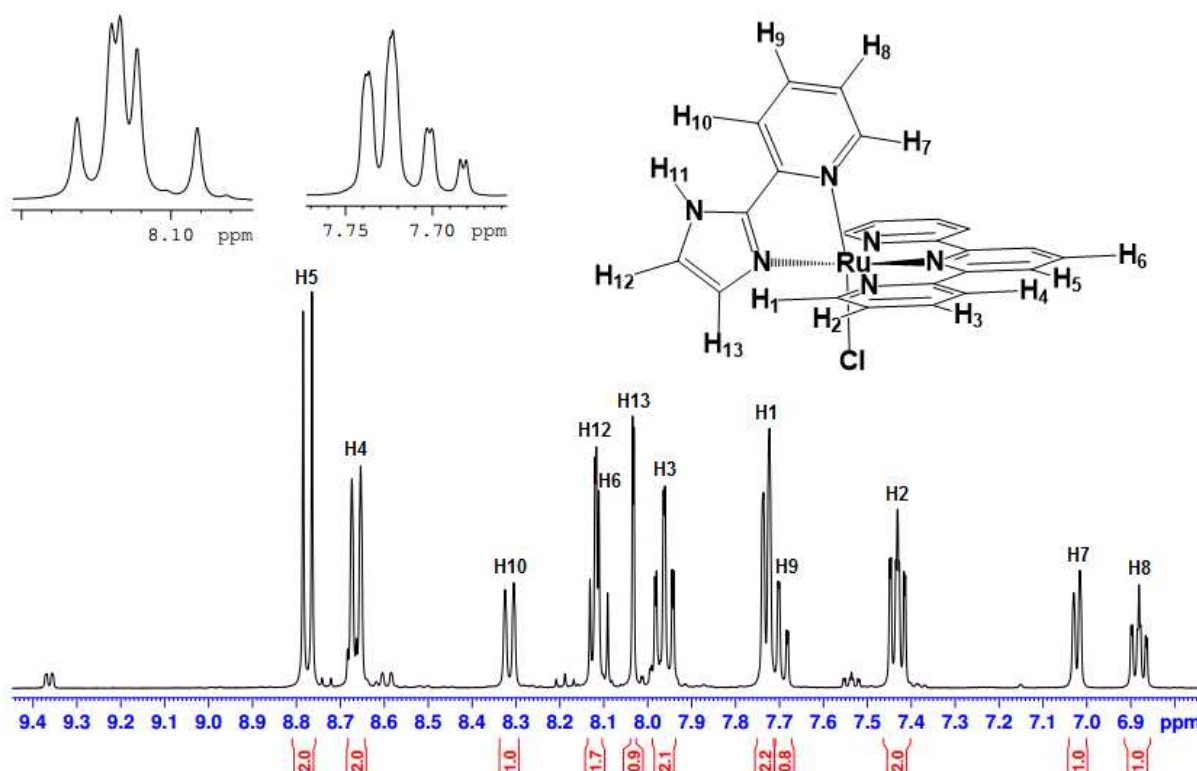


Figure 25: $^1\text{H-NMR}$ spectrum of $[\text{RuCl}(\text{Himpy})(\text{tpy})]\text{Cl}$ in DMSO-d_6 .

The missing hydrogen is the one attached to the imidazole nitrogen, and this probably happens because there is a rapid hydrogen exchange with water present in sample or in deuterated solvent, making the peak resonance of this hydrogen decrease considerably in intensity until it is not seen in the spectrum.

Contrary to expected, H₁ experiences an upfield shift (+1.01 ppm) with respect to free terpyridine, whereas in the case of $[\text{Ru}(\text{tpy})\text{Cl}_3]$ reduced with Zn, it shows a downfield shift (-0.62 ppm). That upfield shift is a consequence of the H₁ environment in the complex as it lies over the π electron cloud of the imidazole moiety. H₅ and H₆ are also deshielded, displaying inductive effects are predominant

over π backdonation. This is supported by crystal structure of the complex, wherein bonding distance between Ru(II) and center pyridine moiety (1.941(3) Å) is shorter than the other two pyridine moieties (2.045(3) and 2.063(3) Å), strengthening electron donation of the nitrogen to the metal center. The same pattern is observed for the Himpy ligand, being H₇, H₈ and H₉ shielded as a consequence of lying over the π electron cloud of the terpyridine moiety, whereas H₁₀, H₁₂ and H₁₃ are deshielded because of they are out of that shielding region.

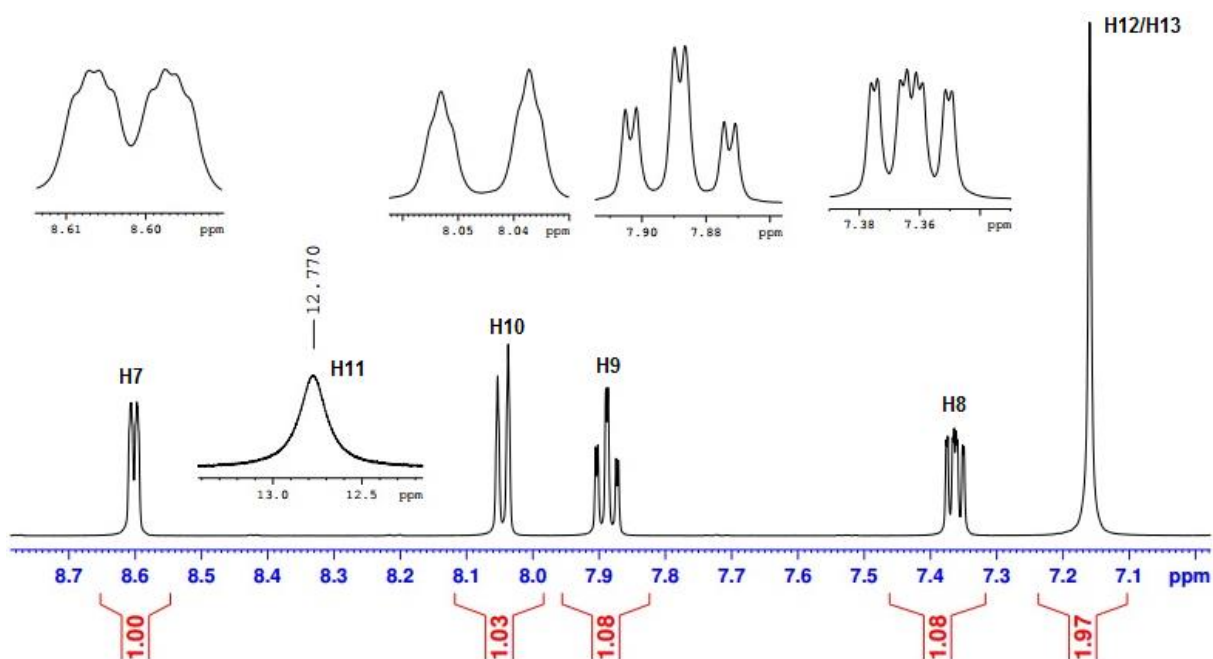


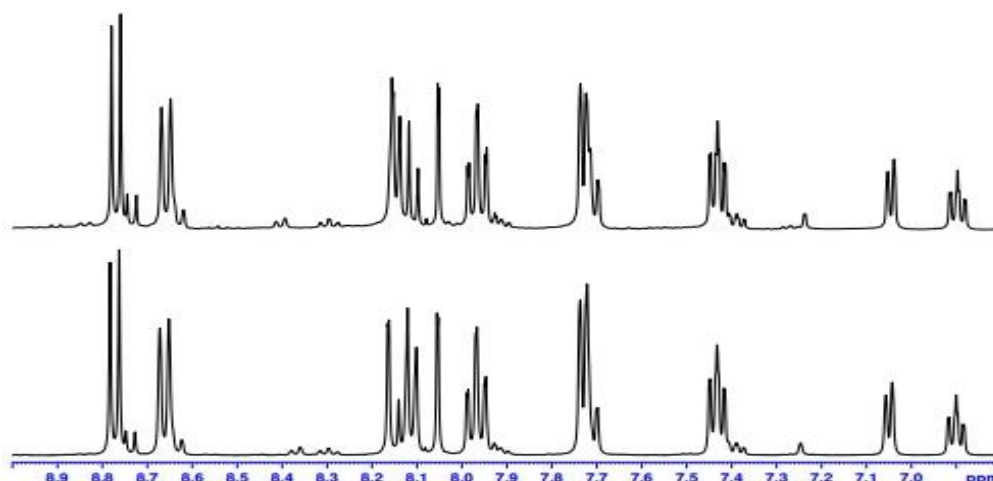
Figure 26: ¹H-NMR spectrum of free Himpy ligand in DMSO-d₆.

Furthermore, hydrogens H₁₂ and H₁₃ experience the same chemical shift in free Himpy ligand, but upon coordination one of them is more deshielded than the other since it is further from terpyridine shielding region. The signal assignments, splitting pattern, chemical shifts and proton-proton coupling constants for [RuCl(Himpy)(tpy)]⁺ complex are shown in **Table 7**.

Table 7: $^1\text{H-NMR}$ data for $[\text{RuCl}(\text{Himpy})(\text{tpy})]\text{Cl}$ recorded in DMSO-d_6 .

Hydrogen	Splitting pattern	Integration	δ (ppm)	J (Hz)
H5	d	2	8.77	8.0
H4	d	2	8.66	8.0
H10	d	1	8.31	7.8
H12	d	1	8.12	1.0
H6	t	1	8.11	8.0
H13	d	1	8.03	1.0
H3	td	2	7.96	7.8, 1.4
H1	d	2	7.73	5.5
H9	td	1	7.72	7.8, 1
H2	ddd	2	7.43	7.8, 5.5, 1.2
H7	d	1	7.02	5.5
H8	ddd	1	6.90	7.8, 5.5, 1

In addition, there are some peaks much less intense than those related to the complex lying in the aromatic portion of the spectrum due to impurities not removed upon crystallization. First of all, it was thought they were signals of free terpyridine and Himpy ligands, but checking their $^1\text{H-NMR}$ spectra in the same deuterated solvent and comparing to the complex spectrum, that hypothesis was ruled out. Since chloride is found to be a labile ligand,⁸³ it was acquired a $^1\text{H-NMR}$ spectrum of a fresh $[\text{RuCl}(\text{Himpy})(\text{tpy})]\text{PF}_6$ (proton chemical shifts were not altered when counter-ion was changed) compound solution in order to avoid its dissociation from coordination sphere, but those signals not linked to complex were still remained. In order to rule out chloride dissociation from the complex, a $^1\text{H-NMR}$ spectrum of the same complex solution was acquired after one month (**Figure 27**) to check if those impurities and complex proton signals vary in intensity.

**Figure 27:** $^1\text{H-NMR}$ spectrum of a fresh solution (below) and one-month later (above) in DMSO-d_6 .

As can be seen, no changes in signal intensities are observed in one-month later spectrum, discarding chloride dissociation assumption. Constable and Hannon⁸⁴ reported the formation of $[\text{Ru}(\text{tpy})_2]^{2+}$ as an impurity on synthesis of heteroleptic Ru(II) polypyridine complexes using $[\text{Ru}(\text{tpy})\text{Cl}_3]$ as a precursor, so the attention was focused on that possibility. Chemical shift values for $[\text{Ru}(\text{tpy})_2]^{2+}$ protons⁸⁵ were recorded on deuterated acetonitrile, specifically focused on those adjacent to terpyridine nitrogen (H_1) and the one lying in the *para*-position of center pyridine ring (H_6). These protons appear at 7.34 ppm and 8.42 ppm, respectively. As their chemical shifts were obtained in CD_3CN , this solvent was used to acquire a spectrum of the complex (**Figure 28**) in order to check if those signals match the signals impurities.

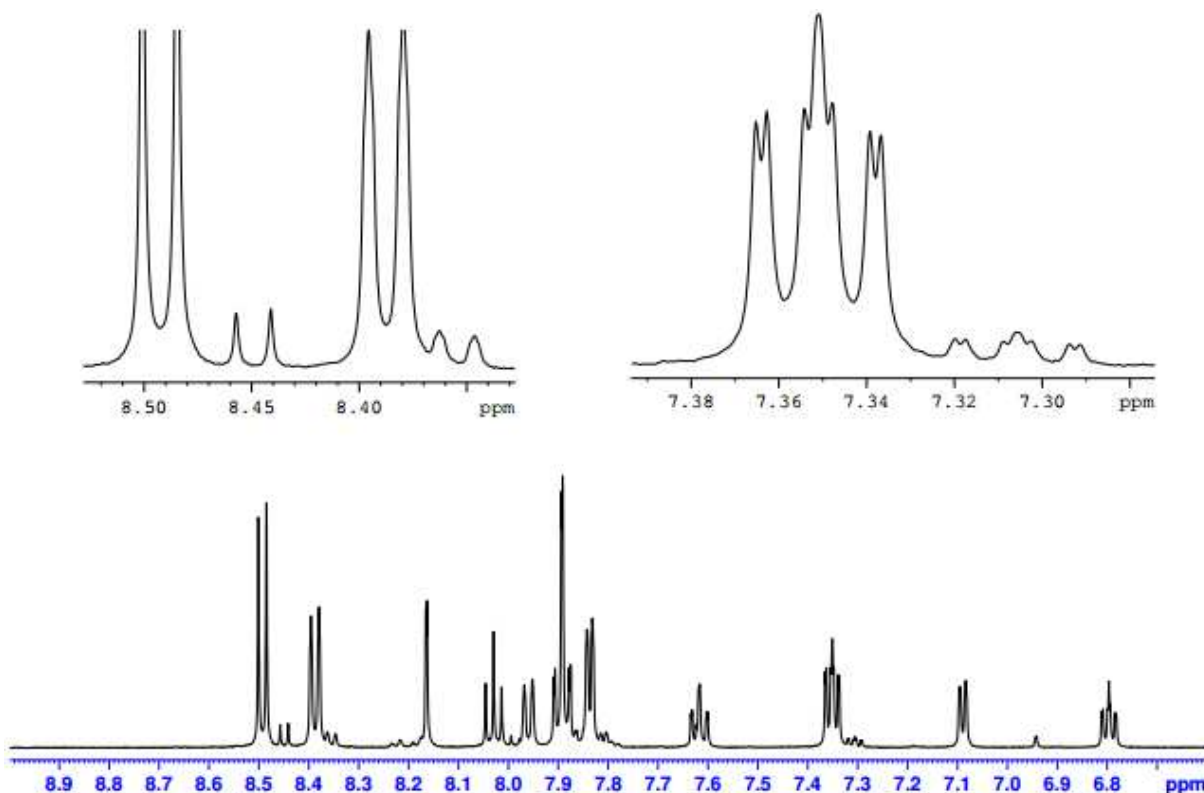


Figure 28: ^1H -NMR spectrum of $[\text{RuCl}(\text{Himpy})(\text{tpy})]^+$ complex in CD_3CN .

The mentioned protons H_1 and H_6 show doublet (d) and triplet (t) splitting patterns, respectively. The spectrum exhibits two signals close to 7.34 ppm and 8.42 ppm, but multiplicity of those proton signals, doublet of doublet of doublets (ddd) and doublet (d), do not match the expected ones, concluding the impurities are not subjected to $[\text{Ru}(\text{tpy})_2]^{2+}$ complex.

The possibility of an isomer, whose structure contains the pyridine ring in a trans position to terpyridine ring, was also taken into consideration, but crystals of the complex after slow evaporation from acetonitrile solution gave rise to one crystal structure, as shown in **Figure 29**.

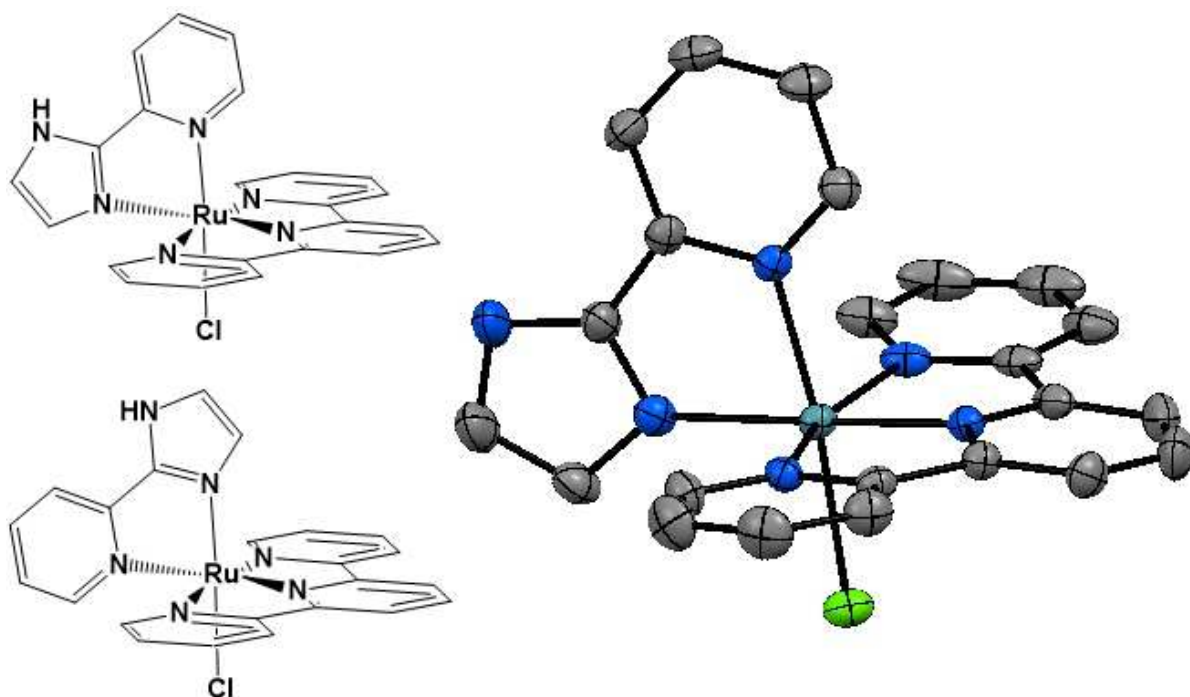


Figure 29: Possible isomers and crystal structure of $[\text{RuCl}(\text{Himpy})(\text{tpy})]^+$ complex.

This result could have led us to discard the possibility of an isomer. But at making a zoom on those impurities, they displayed the same splitting patterns and ratios as the signals for the $[\text{RuCl}(\text{Himpy})(\text{tpy})]^+$ complex (**Figure 30**).

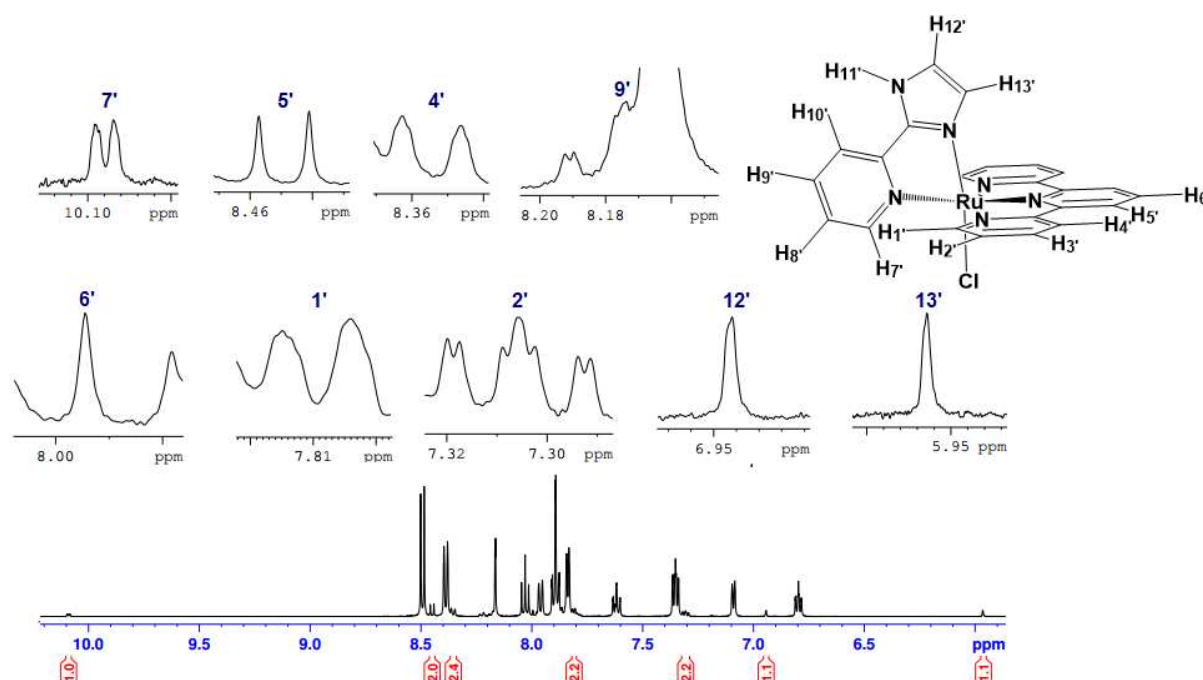


Figure 30: Zoom on impurities signals of $^1\text{H-NMR}$ spectrum of $[\text{RuCl}(\text{Himpy})(\text{tpy})]^+$ complex in CD_3CN .

In this case, pyridine ring is in a cis position to chloride ligand. It is observed that now imidazole ring is above the pi cloud region of terpyridine, so pyridine hydrogens are deshielded and imidazole hydrogens are shielded as confirmed by $^1\text{H-NMR}$ data presented in **Table 8**. These data were compared to those for $[\text{RuCl}(\text{bpy})(\text{tpy})]\text{PF}_6$ ($^1\text{H-NMR}$ data in CD_3CN) because there are two pyridine rings that are cis and trans to chloride, being one of them above the pi cloud region of terpyridine, so it could be compared to our case.

Table 8: $^1\text{H-NMR}$ data for $[\text{RuCl}(\text{bpy})(\text{tpy})]\text{PF}_6$ (**1**),⁸⁴ isomer of $[\text{RuCl}(\text{Himpy})(\text{tpy})]\text{PF}_6$ (**2**) and free ligand Himpy (**3**) (in DMSO-d_6).

Hydrogen	δ (ppm) (1)	δ (ppm) (2)	δ (ppm) (3)
7' (py)	10.20	10.10	8.59
8'	7.95	Not shown	7.35
9'	8.25	8.17	7.88
10'	8.58	Not shown	8.04
12' (Him)	-	6.94	7.16
13'	-	5.96	7.16
1' (tpy)	7.66	7.81	-
2'	7.26	7.30	-
3'	7.88	Not shown	-
4'	8.37	8.35	-
5'	8.49	8.45	-
6'	8.09	7.99	-

So based on these data, we could say those impurities are related to an isomer, wherein pyridine ring now is in a trans position to terpyridine ring. The fact the crystals were related to just one isomer could be due to the isomers ratio (8:1), as shown in **Figure 31**.

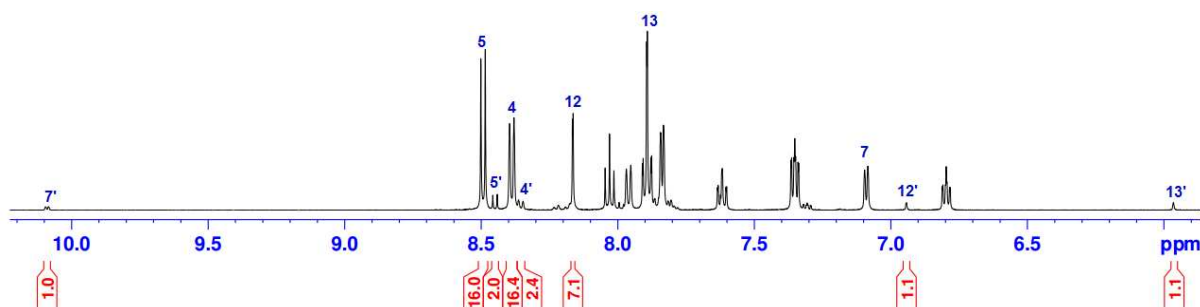


Figure 31: $^1\text{H-NMR}$ spectrum of $[\text{RuCl}(\text{Himpy})(\text{tpy})]^+$ complex in CD_3CN showing the isomers ratio.

TLC plates were performed in order to investigate the adequate solvent to separate them. It was tested cyclohexane, chloroform, acetone, acetonitrile, ethanol, methanol and water. The spots loaded on TLC plates just eluted with high polar solvents ethanol, methanol and water, while on the other solvents they remained at the baseline. It was also tried with mixtures of ethanol and methanol with water in order to see if they could separate, but there were not satisfactory results (**Figure 32**).

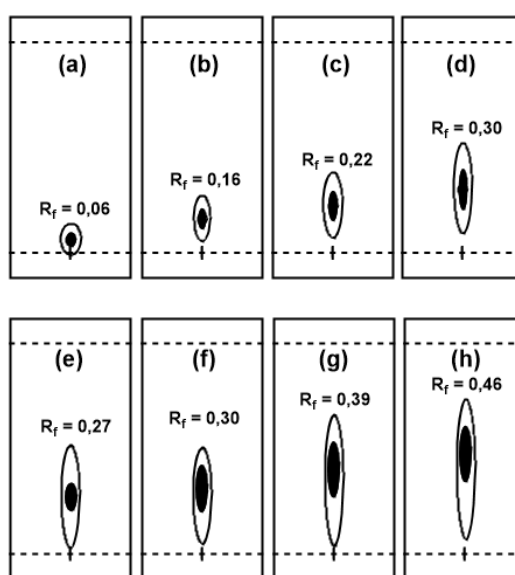


Figure 32: TLC plates in a) pure methanol and mixtures of methanol:water b) 9:1, c) 8:2, d) 7:3 as well as in ethanol:water e) 9:1, f) 8:2, g) 6:4, h) 1:1.

All the other Ru(II) complexes were also characterized by $^1\text{H-NMR}$ spectroscopy. Their $^1\text{H-NMR}$ spectra show resonance proton signals in agreement with their structures, and those related to precursor impurities. Proton chemical shifts for $[\text{RuCl}(\text{Himpa})(\text{tpy})]^+$ complex are listed in **Table 9**. It is also shown for free tpy (H_1 - H_6) and Himpa (H_7 - H_{12}) ligands for comparison purposes. It is worth mentioning that $^1\text{H-NMR}$ spectrum of the complex was obtained after performing column chromatography, using neutral alumina and $\text{CH}_3\text{OH}:\text{CH}_2\text{Cl}_2$ 1:10 as the stationary phase and mobile phase, respectively.

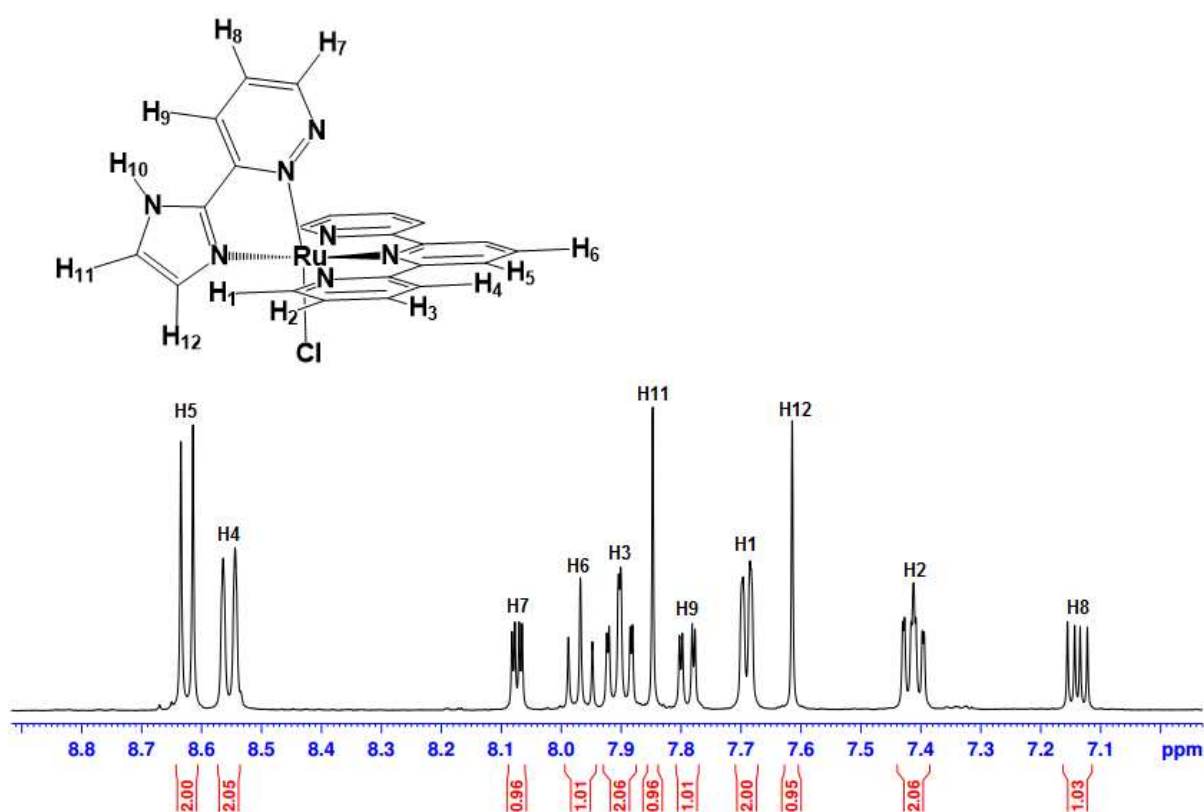


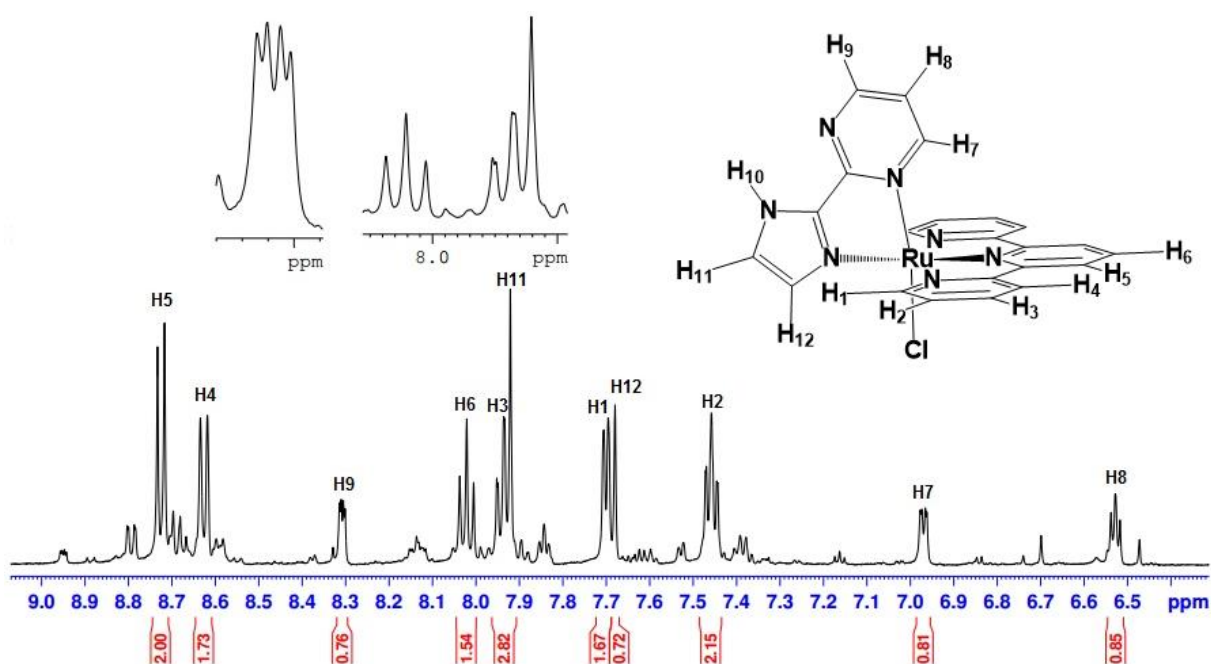
Figure 33: $^1\text{H-NMR}$ spectrum of the $[\text{RuCl}(\text{Himpa})(\text{tpy})]^+$ complex in DMSO-d_6 .

As obtained for the previous $[\text{RuCl}(\text{Himpy})(\text{tpy})]^+$ complex, pyridazine hydrogens H_7 , H_8 and H_9 experience an upfield shift compared to free ligand, while imidazole hydrogens H_{11} and H_{12} are deshielded, experiencing the latter less downfield. That behavior leads to suppose a similar structure to previous complex containing Himpy ligand.

Table 9: $^1\text{H-NMR}$ data for $[\text{RuCl}(\text{Himpa})(\text{tpy})]^+$ complex and ligands.

Hydrogen	Ligand	$[\text{RuCl}(\text{Himpa})(\text{tpy})]^+$
H1	8.74	7.69
H2	7.51	7.41
H3	8.03	7.90
H4	8.64	8.55
H5	8.46	8.62
H6	8.12	7.97
H7	9.20	8.07
H8	7.79	7.14
H9	8.24	7.79
H10	13.34	-
H11	7.23	7.85
H12	7.32	7.41

$^1\text{H-NMR}$ spectrum of the $[\text{RuCl}(\text{Himp}) (\text{tpy})]^+$ complex without purification was acquired, showing not only proton signals corresponding to proposed structure, but also several unknown impurities.

**Figure 34:** $^1\text{H-NMR}$ spectrum of the $[\text{RuCl}(\text{Himp})(\text{tpy})]^+$ complex in DMSO-d_6 .

Proton chemical shifts for $[\text{RuCl}(\text{Himp})(\text{tpy})]^+$ complex are listed in **Table 10**. It is also shown for free tpy ($\text{H}_1\text{-H}_6$) and Himpm ($\text{H}_7\text{-H}_{12}$) ligands for comparison purposes. Pyrimidine hydrogens H_7 , H_8 and H_9 experience an upfield shift compared to free ligand, being H_7 most shielded, while imidazole hydrogens H_{11} and H_{12} are

deshielded, experiencing the latter less downfield. That behavior leads to suppose a similar structure to previous complex containing Himpy ligand.

Table 10: $^1\text{H-NMR}$ data for $[\text{RuCl}(\text{Himpm})(\text{tpy})]^+$ complex and ligands.

Hydrogen	Ligand	$[\text{RuCl}(\text{Himpm})(\text{tpy})]^+$
H1	8.74	7.70
H2	7.51	7.46
H3	8.03	7.93
H4	8.64	8.63
H5	8.46	8.72
H6	8.12	8.02
H7	8.88	6.97
H8	7.44	6.53
H9	8.88	8.31
H10	13.09	-
H11	7.26	7.92
H12	7.26	7.68

$^1\text{H-NMR}$ spectrum of the $[\text{RuCl}(\text{Himpz})(\text{tpy})]^+$ complex without purification was acquired, showing not only proton signals corresponding to proposed structure, but also signals that are likely due to remained precursor complex.

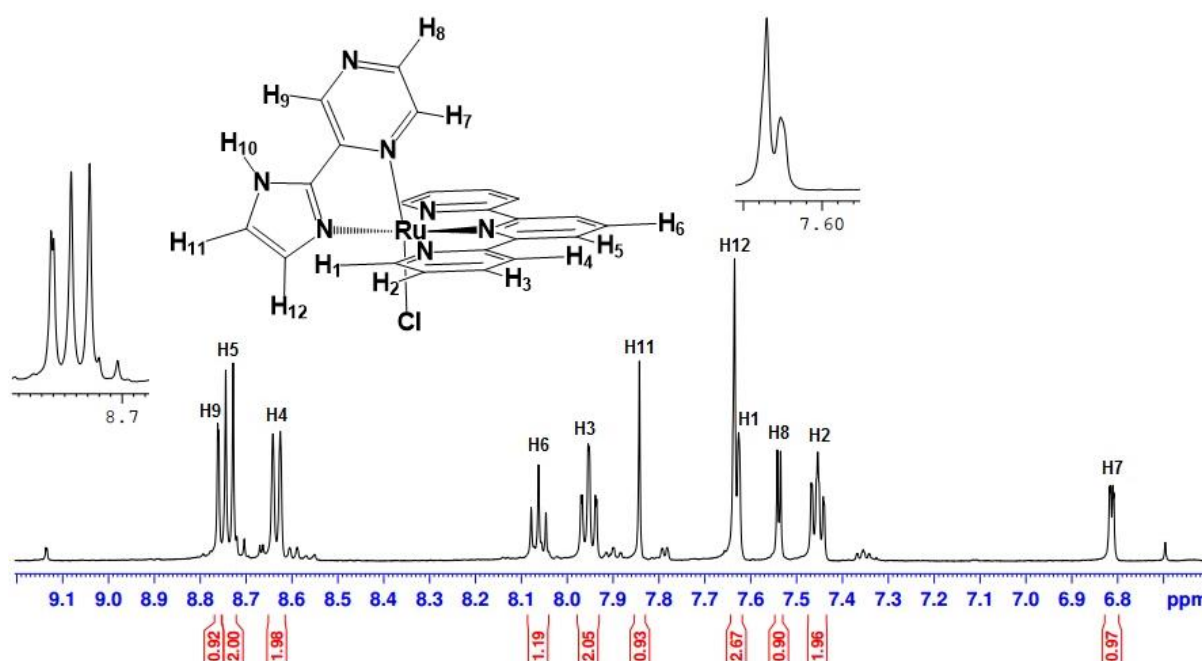


Figure 35: $^1\text{H-NMR}$ spectrum of the $[\text{RuCl}(\text{Himpz})(\text{tpy})]^+$ complex in DMSO-d_6 .

Proton chemical shifts for $[\text{RuCl}(\text{Himpz})(\text{tpy})]^+$ complex, free tpy (H1-H6) and Himpz (H7-H12) ligands for comparison purposes, are listed in **Table 11**.

Pyrazine hydrogens H₇, H₈ and H₉ experience an upfield shift compared to free ligand, being H₇ most shielded, while imidazole hydrogens H₁₁ and H₁₂ are deshielded, being H₁₂ least downfield shifted.

Table 11: ¹H-NMR data for [RuCl(Himpz)(tpy)]⁺ complex and ligands.

Hydrogen	Ligand	[RuCl(Himpz)(tpy)] ⁺
H1	8.74	7.63
H2	7.51	7.45
H3	8.03	7.95
H4	8.64	8.63
H5	8.46	8.74
H6	8.12	8.06
H7	8.88	6.81
H8	7.44	7.54
H9	8.88	8.76
H10	13.09	-
H11	7.26	7.84
H12	7.26	7.64

X-ray suitable crystals of [RuCl(Himpz)(tpy)]PF₆ compound were obtained through slow evaporation from its acetonitrile solution and crystal structure (**Figure 36**) confirms the presence of one isomer with the pyrazine moiety involved in coordination to Ru(II) center.

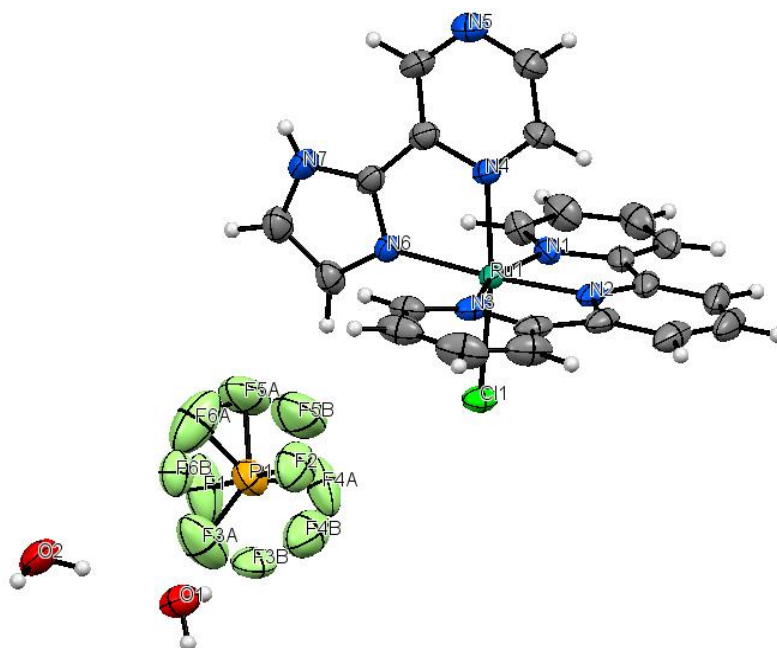


Figure 36: ORTEP view of the X-ray structure of [RuCl(Himpz)(tpy)]PF₆·2H₂O at 150K.

In the structure, Ru(II) ion is coordinated to Himpz, tpy and chloride ligands in a distorted octahedral geometry. The chloride ligand is trans to the pyrazyl nitrogen atom of the heteroaryl imidazole moiety. The terpyridine moiety coordinates in a *mer* fashion and the Himpz ligand coordinates in a perpendicular position (89.20°) relative to the planar terpyridine moiety. Cl1-Ru(II)-N4 angle ($172.11(7)^\circ$) is slightly different from the 180° angle for a octahedral geometry. It is also observed the bite angle ($78.61(9)^\circ$) of the Himpz ligand. Crystallographic data for the complex are listed in **Table 12**.

Table 12: Crystallographic data for the complex [RuCl(Himpz)(tpy)]PF₆.2H₂O.

Parameter	Compound
Empirical formula	C ₂₂ H ₂₁ N ₇ ClF ₆ O ₂ PRu
Fw	696.95
Crystal symmetry	Monoclinic
Space group	P 2 ₁ /c
a (Å)	13.7919(13)
b (Å)	12.7284(12)
c (Å)	16.0132(15)
α, γ (°)	90.00
β (°)	113.632(2)
V (Å³)	2575.4(4)
Z	4
T (K)	150

4.6 Electrochemistry of the complexes

Electrochemical measurements were performed in acetonitrile solutions to determine redox behavior of the complexes. Electrochemical data for redox couple Ru(II)/Ru(III) complexes are listed on **Table 13**. The potentials of the complexes against Fc/Fc⁺ couple were obtained by making cyclic voltammetry of Fc/Fc⁺ couple against Ag/AgNO₃ and then subtracting their potentials.

Table 13: Electrochemical data of [RuCl(L)(tpy)]⁺ complexes in acetonitrile. Potentials against reference electrodes are given in volts (V).

Complex	vs. Ag/AgNO ₃	vs. Fc/Fc ⁺	vs. NHE ⁸⁶	ΔE _p (mV)
[RuCl(Himpy)(tpy)] ⁺	0.40	0.26	0.94	80.5
[RuCl(Himpa)(tpy)] ⁺	0.45	0.31	0.99	80.5
[RuCl(Himpm)(tpy)] ⁺	0.46	0.32	1.00	95.7
[RuCl(Himpz)(tpy)] ⁺	0.50	0.36	1.04	75.5

Cyclic voltammograms (**Figure 37**) show some values ranging from 0.40 V to 0.50 V vs. Ag/AgNO₃ corresponding to reversible oxidation process of Ru(II) to Ru(III) in all the [RuCl(L)(tpy)]⁺ complexes. All those Ru(II)/Ru(III) oxidation potentials are cathodically shifted compared to [RuCl(bpy)(tpy)]⁺ (0.42 V vs. Fc/Fc⁺),⁸⁴ which is consistent by virtue of they containing a more electron releasing imidazol ring instead of a pyridine. As can be seen, there are other peaks at higher potential values that could be related to the isomer in lower proportion, but this needs to be confirmed by performing further electrochemical experiments.

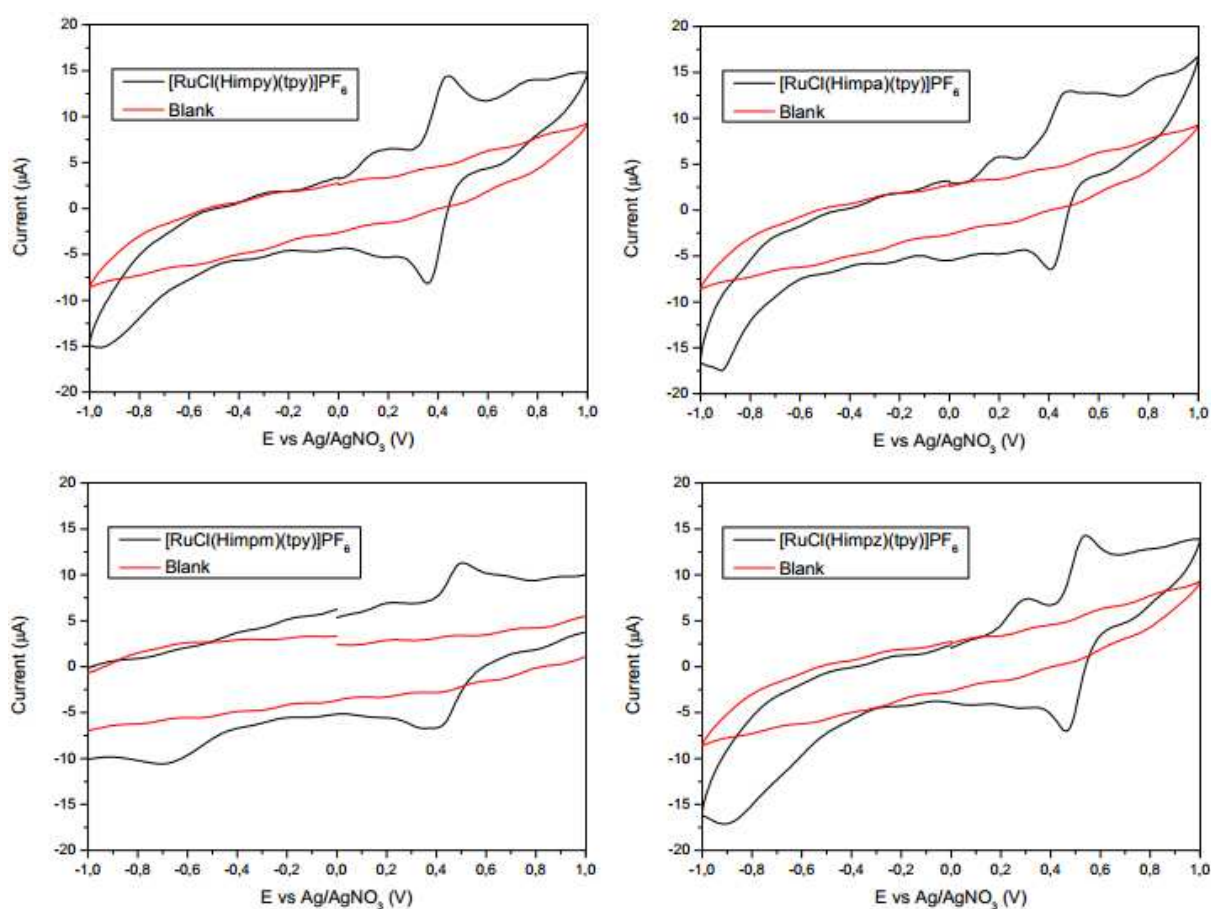


Figure 37: Cyclic voltammograms of the Ru²⁺ complexes (2×10^{-3} mol L⁻¹) in TBAPF₆ (0.1 mol L⁻¹ in CH₃CN). Scan rate: 0.1V/s.

[RuCl(Himpz)(tpy)]⁺ complex exhibits most positive oxidation potential whereas [RuCl(Himpy)(tpy)]⁺ complex shows the lowest value. Based on crystal structures obtained in this work, those potentials seem to be influenced by both the basicity of the heteroaryl and imidazole rings, which are involved in coordination to Ru(II) ion. The pK_a measurements for heteroaryl-2-imidazole ligands were performed

in aqueous solutions. **Table 14** shows pK_a contributions from both heteroaryl and imidazole rings, being imidazole nitrogen from heteroaryl-2-imidazole ligand involved in protonation (**Figure 38**). The close values of potentials are related to the basicity of heteroaryl-2-imidazole ligands, which are also close among them. Nevertheless, the order of potential values is not directly related to those basicities. However, it is observed the direct relationship between oxidation potentials and basicity of heteroaryl rings. Pyrazine ($pK_a = 0.6$) has the lowest basicity among the other heteroaryl rings pyrimidine ($pK_a = 1.3$), pyridazine ($pK_a = 2.3$) and pyridine ($pK_a = 5.2$).⁴⁰ So it can be supposed the potentials are directly influenced by the total contribution of both heteroaryl and imidazole basicities.

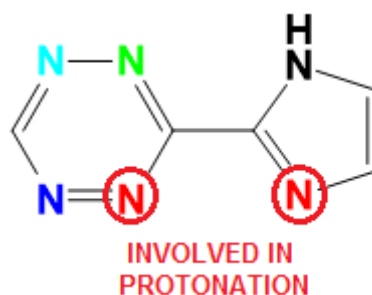


Figure 38: Nitrogen atoms involved in protonation.

Table 14: Oxidation potentials of $[RuCl(L)(tpy)]^+$ complexes and pK_a values of heteroaryl and heteroaryl-2-imidazole rings.

Complex	E°_{ox}	pK_a	
		Heteroaryl ⁴⁰	Heteroaryl-2-imidazole
$[RuCl(Himpy)(tpy)]^+$	0.40	5.2	5.51
$[RuCl(Himpa)(tpy)]^+$	0.45	2.3	4.29
$[RuCl(Himpm)(tpy)]^+$	0.46	1.3	5.13
$[RuCl(Himpz)(tpy)]^+$	0.50	0.6	4.58

4.7 Electronic properties of the complexes

The electronic absorption spectra of the ruthenium(II) complexes in acetonitrile in the 200-800 nm range are represented in **Figure 39**. All the complexes show intense absorption bands in the 200-350 nm region which are related to ligand centered $\pi \rightarrow \pi^*$ transitions.⁸⁷ Broad bands are also observed in the 400-600 nm region which could be result of overlapping metal-to-ligand charge-transfer (MLCT) transitions $d\pi^6 (Ru) \rightarrow \pi^* (tpy, L)$,^{71,87} being L the heteroaryl-2-imidazol ligand.

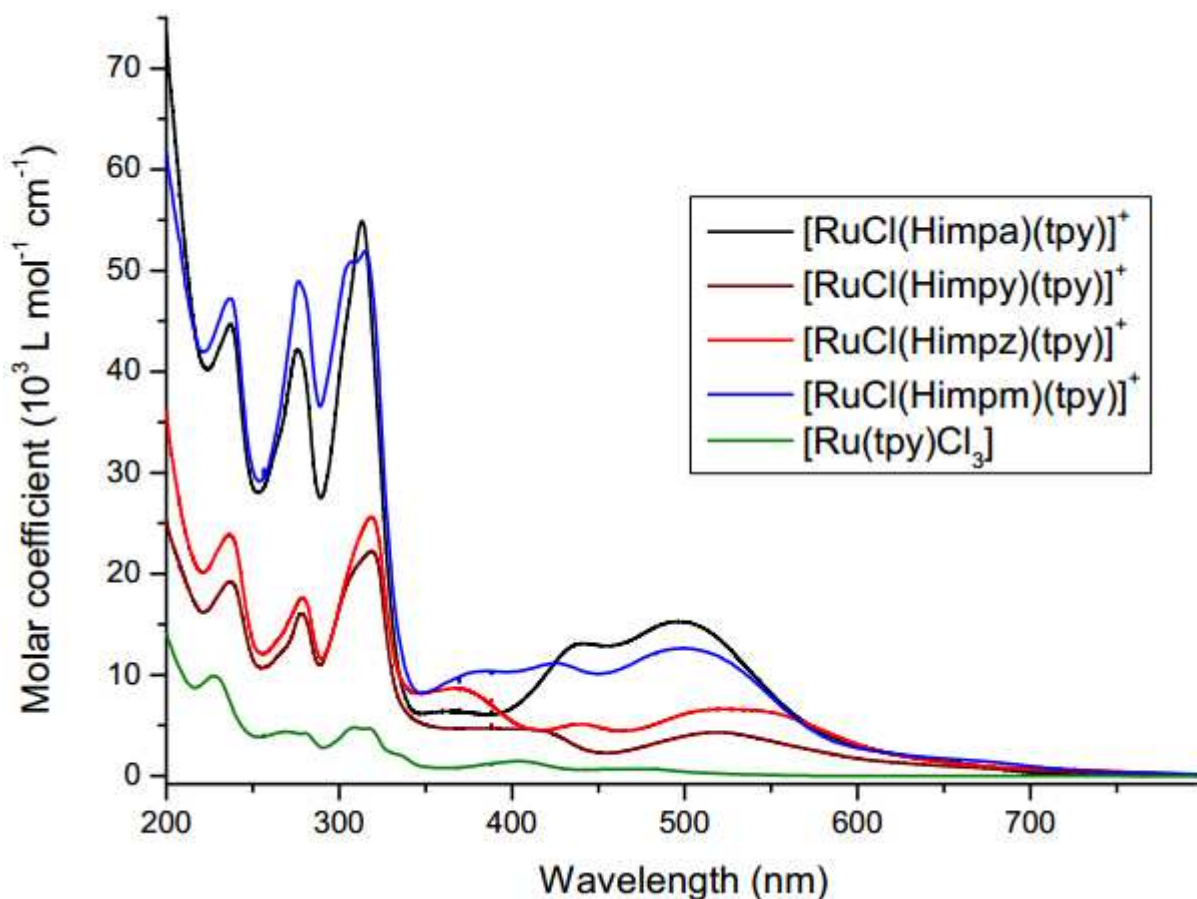


Figure 39: Electronic absorption spectra of the Ru(II) complexes in acetonitrile.

The spectral data is given in **Table 15**. All MLCT bands in the four complexes $[\text{RuCl}(\text{L})(\text{tpy})]^+$ are red shifted compared to $[\text{Ru}(\text{tpy})_2]^{2+}$ whose MLCT band is observed at around 475 nm.⁷³ The shift to lower energy could be explained taking into account the chloride ligand is a better π donor than pyridine,⁸⁸ resulting in a destabilization of the ruthenium t_{2g} orbital whose energy arises. There is also an imidazol moiety ($\text{pK}_a = 7.05$),⁸⁹ a better σ donor than pyridine ($\text{pK}_a = 5.23$),⁴⁰ increasing the e_g^* orbital energy. This seems to have less influence than increase of t_{2g} energy on MLCT energies.

Table 15: Electronic absorption data for the Ru(II) complexes in acetonitrile.

Complex	Wavelength (nm)	ϵ ($10^3 \text{ L mol}^{-1} \text{ cm}^{-1}$)	Assignment
[RuCl(Himpy)(tpy)] ⁺	237	19.3	$\pi \rightarrow \pi^*$
	278	16.2	$\pi \rightarrow \pi^*$
	318	22.5	$\pi \rightarrow \pi^*$
	518	4.3	MLCT
[RuCl(Himpa)(tpy)] ⁺	237	46.6	$\pi \rightarrow \pi^*$
	276	43.9	$\pi \rightarrow \pi^*$
	313	57.3	$\pi \rightarrow \pi^*$
	496	15.9	MLCT
[RuCl(Himpm)(tpy)] ⁺	237	47.5	$\pi \rightarrow \pi^*$
	276	49.2	$\pi \rightarrow \pi^*$
	315	52.4	$\pi \rightarrow \pi^*$
	502	12.7	MLCT
[RuCl(Himpz)(tpy)] ⁺	237	23.8	$\pi \rightarrow \pi^*$
	278	17.6	$\pi \rightarrow \pi^*$
	318	25.7	$\pi \rightarrow \pi^*$
	522	6.6	MLCT

The MLCT band in complex [RuCl(Himpz)(tpy)]⁺ is the most red shifted among the all four complexes, whereas [RuCl(Himpa)(tpy)]⁺ shows the MLCT band at higher energy than the others. Half-wave potentials for one-electron reduction of the heteroaryl ligands pyridine (-2.09 V), pyrimidine (-1.78 V), pyridazine (-1.60 V), and pyrazine (-1.57 V) were reported by Ford and co-workers.⁹⁰ Those values are related to the their LUMO energy, and taking into account the half-wave potentials for Ru(II)/Ru(III) oxidation performed in this work, there is no correlation with MLCT band energies (**Table 16**), maybe because either the LUMO energies for the heteroaryl-2-imidazol ligands do not follow the same pattern as the heteroaryl ligands or if the pattern is followed, their contributions to the LUMO energy of the complex are different compared to that of the terpyridine.⁹¹

Table 16: LUMO energies of heteroaryl rings, HOMO and MLCT energies of Ru(II) complexes.

Complex	LUMO (V)	HOMO (V)	LUMO-HOMO (V)	MLCT (nm)
[RuCl(Himpy)(tpy)] ⁺	-2.09	0.40	2.49	518
[RuCl(Himpm)(tpy)] ⁺	-1.78	0.46	2.24	502
[RuCl(Himpz)(tpy)] ⁺	-1.57	0.50	2.07	522
[RuCl(Himpa)(tpy)] ⁺	-1.60	0.45	2.05	496

4.8 Conductivity measurements of the films

Corrêa and co-workers⁹² described the modification of the surface of glassy carbon electrode with carbon nanotubes dispersed into the metallopolymer P4VP-Fe(CN)₅. In that work, they showed the L-cysteine electrooxidation at low overpotential compared to bare glassy carbon electrode, demonstrating good performance through modification of surface. In this section, we wish to show that semiconductor characteristic of carbon nanotubes is maintained after their dispersion into the metallopolymer, ensuring a good communication between electrode surface and redox active site (pentacyanoferrate complex). This was possible by performing conductivity measurements of the MWCNT/P4VP and MWCNT/P4VP-Fe(CN)₅ films.

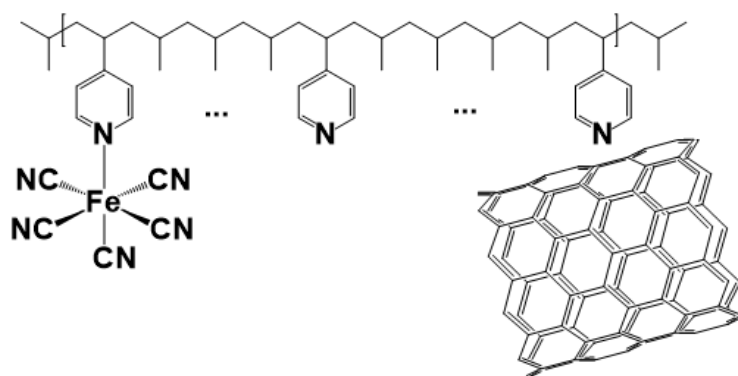


Figure 40: Representative part of the carbon nanotubes dispersed into the metallopolymer P4VP/Fe(CN)₅. Adapted from Corrêa et al.⁹²

The results showed ohmic behavior of both MWCNT/P4VP and MWCNT/metallopolymer films. The values of conductivity were 2.35 and 0.95 mS m⁻¹ respectively, whereas the pure P4VP is known to be an insulator ($\sigma=3.6 \mu\text{S m}^{-1}$).⁹³ The presence of pentacyanoferrate did not change the semiconductor characteristic of the film, which is a property provided by the dispersed MWCNT. The enhanced conductivity of this nanocomposite films combined with the electrocatalytic properties of the pentacyanoferrate have been explored to produce a superior electrochemical sensor for cysteine.⁹² It is worth noting that it was used an iron complex instead of a ruthenium complex because by that time pentacyanoferrate was already synthesized and available, and it was desirable not only obtaining the conductivity of the nanocomposite films but also getting knowledge about the preparation of the films.

5. Conclusions

In summary, it was synthesized the new ligand 3-(1H-imidazol-2-yl)pyridazine and well characterized. $^1\text{H-NMR}$ revealed the presence of six hydrogens, one of them attached to the imidazole nitrogen atom. $^{13}\text{C-NMR}$, 2D $^1\text{H-}^{13}\text{C-HSQC}$ and $^1\text{H-}^{13}\text{C-HMBC}$ also confirmed the proposed structure. Elemental analysis, X-ray crystallography and ESI-MS confirmed the identity of the ligand as well. It was also synthesized the four Ru(II) complexes containing terpyridine and heteroaryl imidazole ligands, as confirmed by ESI-MS and conductivity measurements showing the complex:counter-ion 1:1 composition. Nevertheless, it should be also mentioned that there were some problems related to the compounds purity, as it is shown by $^1\text{H-NMR}$ spectroscopy displaying the presence of the isomer of the complexes. It is worth mentioning that X-ray diffraction revealed the proposed structure of the compound $[\text{RuCl}(\text{Himpz})(\text{tpy})]\text{PF}_6$. The oxidation potentials of the complexes are low, making them useful for applications such as modification of surface electrodes. Therefore, the next steps will be focused on the separation of the mentioned complexes and their isomers and subsequent applications.

6. References

1. Meyer, T. J. Photochemistry of metal coordination complexes: metal to ligand charge transfer excited states. *Pure Appl. Chem.* **58**, 1193–1206 (1986).
2. Crosby, G. & Demas, J. Quantum efficiencies on transition metal complexes. II. Charge-transfer luminescence. *J. Am. Chem. Soc.* **72**, 2841–2847 (1971).
3. Guillerez, S. *et al.* Photoinduced Processes in Dyads and Triads Containing a Ruthenium(II)-Bis(terpyridine) Photosensitizer Covalently Linked to Electron Donor and Acceptor Groups. *Inorg. Chem.* **30**, 4230–4238 (1991).
4. Kalyanasundaram, K., Gratzel, M. & Nazeeruddin, K. Luminescence and Intramolecular Energy-Transfer Processes in Isomeric Cyano-Bridged Rhenium(I)-Rhenium(I) and Rhenium(I)-Ruthenium(II)-Rhenium(I) Polypyridyl Complexes. *Inorg. Chem.* **31**, 5243–5253 (1992).
5. Wasielewski, M. R., M, D. A. & Introducth, I. Photoinduced Electron Transfer in Supramolecular Systems for Artificial Photosynthesis. *Chem. Rev.* **92**, 435–461 (1992).
6. Sauvage, J., Collin, J., Chambron, J. & Guillerez, S. Ruthenium(II) and Osmium(II) Bis(terpyridine) Complexes in Covalently-Linked Multicomponent Systems: Synthesis, Electrochemical Behavior, Absorption Spectra, and Photochemical and Photophysical Properties. *Chem. Rev.* **94**, 993–1019 (1994).
7. Balzani, V., Juris, A., Venturi, M., Campagna, S. & Serroni, S. Luminescent and Redox-Active Polynuclear Transition Metal Complexes †. *Chem. Rev.* **96**, 759–833 (1996).
8. Du, H. & Bossmann, S. Ruthenium Polypyridine Complexes. On the Route to Biomimetic Assemblies as Models for the Photosynthetic Reaction Center. *Acc. Chem. Res.* **34**, 905–917 (2001).
9. Renouard, T. *et al.* Novel Ruthenium Sensitizers Containing Functionalized Hybrid Tetradentate Ligands: Synthesis, Characterization, and INDO/S Analysis. *Inorg. Chem.* **41**, 367–378 (2002).
10. Meyer, T. J. & Huynh, M. H. V. The Remarkable Reactivity of High Oxidation State Ruthenium and Osmium Polypyridyl Complexes. *Inorg. Chem.* **42**, 8140–8160 (2003).
11. Haga, M. *et al.* Synthesis and Proton-Coupled Electron-Transfer Reaction of Self-Assembled Monolayers of a Ruthenium(II) Complex Containing Tridentate

- 2,6-Bis(benzimidazol-2-yl)pyridine on a Gold Surface: Comparison of Acid/Base Chemistry with Bulk Solution Chemistry. *Inorg. Chem.* **39**, 4566–4573 (2000).
12. Baitalik, S., Flo, U., Paderborn, G., Paderborn, D.- & May, R. V. Mononuclear and Binuclear Ruthenium(II) Complexes Containing 2,2'-Bipyridine or 1,10-Phenanthroline and Pyrazole-3,5-Bis(Benzimidazole). Synthesis, Structure, Isomerism, Spectroscopy, and Proton-Coupled Redox Activity. *Inorg. Chem.* **38**, 3296–3308 (1999).
 13. Saha, D., Das, S., Bhaumik, C., Dutta, S. & Baitalik, S. Monometallic and Bimetallic Ruthenium(II) Complexes Derived from 4,5-Bis(Benzimidazol-2-yl)Imidazole (H₃Imbzim) and 2,2'-Bipyridine as Colorimetric Sensors for Anions: Synthesis, Characterization, and Binding Studies. *Inorg. Chem.* **49**, 2334–2348 (2010).
 14. Bhaumik, C., Das, S., Saha, D., Dutta, S. & Baitalik, S. Synthesis, Characterization, Photophysical, and Anion-Binding Studies of Luminescent Heteroleptic Bis-Tridentate Ruthenium(II) Complexes Based on 2,6-Bis(Benzimidazole-2-yl)Pyridine and 4'-substituted 2,2':6',2'' Terpyridine Derivatives. *Inorg. Chem.* **49**, 5049–5062 (2010).
 15. Maity, D., Das, S., Mardanya, S. & Baitalik, S. Synthesis, Structural Characterization, and Photophysical, Spectroelectrochemical, and Anion-Sensing Studies of Heteroleptic Ruthenium(II) Complexes Derived from 4'-Polyaromatic-Substituted Terpyridine Derivatives and 2,6-Bis(benzimidazol-2-yl)pyridine. *Inorg. Chem.* **52**, 6820–6838 (2013).
 16. Studies, A. Ru(II) and Os(II) Complexes Based on Terpyridyl-Imidazole Ligand Rigidly Linked to Pyrene: Synthesis, Structure, Photophysics, Electrochemistry, and Anion-Sensing Studies. *Inorg. Chem.* **52**, 13941–13955 (2013).
 17. Maity, D., Bhaumik, C., Karmakar, S. & Baitalik, S. Photoinduced Electron and Energy Transfer and pH-Induced Modulation of the Photophysical Properties in Homo- and Heterobimetallic Complexes of Ruthenium(II) and Rhodium(III) Based on a Heteroditopic Phenanthroline – Terpyridine Bridge. *Inorg. Chem.* **52**, 7933–7946 (2013).
 18. Morgan, G. T. & Burstall, F. H. Dehydrogenation of Pyridine by Anhydrous Ferric Chloride. *J. Chem. Soc.* 20–30 (1932).
 19. Brandt, W. W. & Smith, F. Polysubstituted 1,10-Phenanthrolines and

- Bipyridines as Multiple Range Redox Indicators. *Anal. Chem.* **21**, 1313–1319 (1949).
20. Wilkins, D. H. & Smith, F. 2,6-bis(2-pyridyl)pyridine and alkyl derivatives. Their properties in the formation of ferrous and cobaltous colored complex cations. *Anal. Chim. Acta* **9**, 338–347 (1953).
 21. Pflaum, R. T. & Brandt, W. W. Metal-Amine Coordination Compounds. Copper(II) complexes. *J. Am. Chem. Soc.* **76**, 6215–6219 (1955).
 22. Pflaum, R. T. & Brandt, W. W. Metal-Amine Coordination Compounds. Copper(I) Complexes. *J. Am. Chem. Soc.* **77**, 2019–2022 (1955).
 23. Brandt, W. W. & Wright, J. P. The Iron-2,2',2''-Terpyridine System. *J. Am. Chem. Soc.* **76**, 3082–3083 (1954).
 24. Schilt, A. A. & Smith, F. 2,6-bis(4-phenyl-2-pyridyl)-4-phenyl-, and 2,6-bis(6-phenyl-2-pyridyl)-4-phenylpyridine. Their spectrophotometric constants in reactions of chelation with Fe(II), Cu(I) and Co(II). *Anal. Chim. Acta* **15**, 567–572 (1956).
 25. Smith, F. & Banick, M. The Fe(II) and Co(II) chelation complexes of 2,6-bis(4-ethyl-2-pyridyl)-4-phenyl-pyridine. *Anal. Chim. Acta* **18**, 269–271 (1958).
 26. Maestri, M., Armaroli, N., Balzani, V., Constable, E. C. & Thompson, A. M. W. C. Complexes of the Ruthenium(II)-2,2':6',2''-Terpyridine Family. Effect of Electron-Accepting and -Donating Substituents on the Photophysical and Electrochemical Properties. *Inorg. Chem.* **34**, 2767 (1995).
 27. Fang, Y.-Q. *et al.* Ruthenium(II) complexes with improved photophysical properties based on planar 4'-(2-pyrimidinyl)-2,2':6',2''-terpyridine ligands. *Inorg. Chem.* **46**, 2854–2863 (2007).
 28. Winkler, J. R., Netzel, T. L., Creutz, C. & Sutin, N. Direct observation of metal-to-ligand charge-transfer (MLCT) excited states of pentaammineruthenium(II) complexes. *J. Am. Chem. Soc.* **109**, 2381–2392 (1987).
 29. Baranoff, E. *et al.* From ruthenium(II) to iridium(III): 15 years of triads based on bis-terpyridine complexes. *Chem. Soc. Rev.* **33**, 147–155 (2004).
 30. Wang, J., Fang, Y.-Q., Hanan, G. S., Loiseau, F. & Campagna, S. Synthesis and Properties of the Elusive Ruthenium(II) Complexes of 4'-Cyano-2,2':6',2''-terpyridine. *Inorg. Chem.* **44**, 5–7 (2005).
 31. Mamaev, V. P., Shkurko, O. P. & Baram, S. G. Electronic Effects of Heteroaromatic and Substituted Heteroaromatic Groups. *Adv. Heterocycl.*

- Chem.* **42**, 1–82 (1987).
32. Blau, F. Die Destillation pyridinmonocarbonsaurer Salze. *Ber. Dtsch. Chem. Ges.* **27**, 1077–1078 (1888).
 33. Juris, A. *et al.* Ru(II) polypyridine complexes: photophysics, photochemistry, electrochemistry, and chemiluminescence. *Coord. Chem. Rev.* **84**, 85–277 (1988).
 34. Caspar, J. V & Meyer, T. J. Photochemistry of MLCT Excited States. Effect of Nonchromophoric Ligand Variations on Photophysical Properties in the Series *cis*-[Ru(bpy)₂L₂]²⁺. *Inorg. Chem.* **22**, 2444–2453 (1983).
 35. Caspar, J. V & Meyer, T. J. Photochemistry of [Ru(bpy)₃]²⁺. Solvent Effects. *J. Am. Chem. Soc.* **105**, 5583–5590 (1983).
 36. Kalyanasundaram, K. Photophysics and Photoredox Reactions of Ligand-Bridged Binuclear Polypyridyl Complexes of Ruthenium(II) and of Their Monomeric Analogues. *Inorg. Chem.* **29**, 1888–1897 (1990).
 37. Frank, A. J. *et al.* Multimetallic Ruthenium(II) Complexes Based on Biimidazole and Bibenzimidazole: Effect of Dianionic Bridging Ligands on Redox and Spectral Properties. *Inorg. Chem.* **29**, 167–175 (1990).
 38. Rillema, D. P. *et al.* MLCT- π - π^* Energy Gap in Pyridyl-Pyrimidine and Bis(pyridine) Complexes of Ruthenium(II). *Inorg. Chem.* **31**, 1600–1606 (1992).
 39. Hang, M., Huynh, V., Dattelbaum, D. M. & Meyer, T. J. Excited state electron and energy transfer in molecular assemblies. *Coord. Chem. Rev.* **249**, 457–483 (2005).
 40. Albert, A., Goldacre, R. & Phillips, J. The strength of heterocyclic bases. *J. Chem. Soc.* 2240–2249 (1948).
 41. Ernst, S. & Kaim, W. Coordination Characteristics of Four Isomeric α -Diimine Ligands. π Molecular Orbital Perturbation Calculations for the Bidiazines and Their Correlation with the Properties of Group 6 Metal Carbonyl Complexes. *J. Am. Chem. Soc.* **108**, 3578–3586 (1986).
 42. Barigelletti, F., Juris, A., Balzani, V., Belser, P. & Von Zelewsky, A. Influence of the ligand structure on the electrochemical and spectroscopic properties of ruthenium(II)-polypyridine complexes. *Inorg. Chem.* **26**, 4115–4119 (1987).
 43. Crutchley, R. J. & Lever, A. B. P. Ruthenium(II) tris(bipyrazyl) dication - a new photocatalyst. *J. Am. Chem. Soc.* **102**, 7128–7129 (1980).
 44. Kitamura, N., Kawanishi, Y. & Tazuke, S. Spectroscopic and electrochemical

- studies on ruthenium(II) complexes containing diazadiimine ligands. *Chem. Phys. Lett.* **97**, 103–106 (1983).
45. Gerli, A., Reedijk, J., Lakin, M. T. & Spek, A. L. Redox Properties and Electrocatalytic Activity of the Oxo/Aqua System $[\text{Ru}(\text{terpy})(\text{bpz})(\text{O})]^{2+}/[\text{Ru}(\text{terpy})(\text{bpz})(\text{H}_2\text{O})]^{2+}$. X-ray Crystal Structure of $[\text{Ru}(\text{terpy})(\text{bpz})\text{Cl}]\text{PF}_6 \cdot \text{MeCN}$ (terpy = 2,2',2''-Terpyridine; bpz = 2,2'-Bipyrazine). *Inorg. Chem.* **34**, 1836–1843 (1995).
 46. Hage, R., Prins, R., Haasnoot, J. G., Reedijk, J. & Vos, J. G. Synthesis, spectroscopic, and electrochemical properties of bis(2,2'-bipyridyl)-ruthenium compounds of some pyridyl-1,2,4-triazoles. *J. Chem. Soc. Dalton Trans.* 1389 (1987).
 47. Haga, M. A. Synthesis and protonation-deprotonation reactions of ruthenium(II) complexes containing 2,2'-bibenzimidazole and related ligands. *Inorganica Chim. Acta* **75**, 29–35 (1983).
 48. Ghedini, M., Longeri, M. & Neve, F. Platinum(II) dimethyl and diphenyl complexes with some bidiazines and 3,6-bis(2'-pyridyl)pyridazine. *Inorganica Chim. Acta* **132**, 223–228 (1987).
 49. Concepcion, J. J., Tsai, M.-K., Muckerman, J. T. & Meyer, T. J. Mechanism of Water Oxidation by Single-Site Ruthenium Complex Catalysts. *J. Am. Chem. Soc.* **132**, 1545–1557 (2010).
 50. Stefopoulos, A., Pefkianakis, E., Papagelis, K., Andreopoulou, A. & Kallitsis, J. Carbon Nanotubes Decorated with Terpyridine-Ruthenium Complexes. *J. Polym. Sci. Part A Polym. Chem.* **47**, 2551–2559 (2009).
 51. Meyer, J. Chemical Approaches to Artificial Photosynthesis. *Acc. Chem. Res.* **22**, 163–170 (1989).
 52. Iijima, S. Helical microtubules of graphitic carbon. *Lett. to Nat.* **354**, 56–58 (1991).
 53. Sun, Y. P. *et al.* Luminescence anisotropy of functionalized carbon nanotubes in solution. *Chem. Phys. Lett.* **351**, 349–353 (2002).
 54. Huang, W. Z. *et al.* The effect of pretreatments on hydrogen adsorption of multi-walled carbon nanotubes. *Mater. Chem. Phys.* **78**, 144–148 (2003).
 55. Tans, S., Verschueren, A. & Dekker, C. Room-temperature transistor based on a single carbon nanotube. *Nature* **672**, 669–672 (1998).
 56. Balasubramanian, K. & Burghard, M. Chemically functionalized carbon

- nanotubes. *Small* **1**, 180–192 (2005).
57. Huczko, A. Synthesis of aligned carbon nanotubes. *Appl. Phys. A Mater. Sci. Process.* **74**, 617–638 (2002).
 58. Rubianes, M. D. & Rivas, G. A. Dispersion of multi-wall carbon nanotubes in polyethylenimine: A new alternative for preparing electrochemical sensors. *Electrochem. commun.* **9**, 480–484 (2007).
 59. Pompeo, F. & Resasco, D. E. Water Solubilization of Single-Walled Carbon Nanotubes by Functionalization with Glucosamine. *Nano Lett.* **2**, 369–373 (2002).
 60. Holzinger, M. *et al.* Sidewall Functionalization of Carbon Nanotubes. *Angew. Chem. Int. Ed.* **40**, 4002–4005 (2001).
 61. Qin, S., Qin, D., Ford, W. T., Resasco, D. E. & Herrera, J. E. Functionalization of Single-Walled Carbon Nanotubes with Polystyrene via Grafting to and Grafting from Methods. *Macromolecules* **37**, 752–757 (2004).
 62. Khairoutdinov, R. F., Doubova, L. V., Haddon, R. C. & Saraf, L. Persistent Photoconductivity in Chemically Modified Single-Wall Carbon Nanotubes. *J. Phys. Chem. B* **108**, 19976–19981 (2004).
 63. Ajayan, P. M. & Tour, J. M. Materials Science: Nanotube composites. *Nature* **447**, 1066 (2007).
 64. Andrieux, C. P. & Saveant, J. M. Heterogeneous (chemically modified electrodes, polymer electrodes) vs. homogeneous catalysis of electrochemical reactions. *J. Electroanal. Chem. Interfacial Electrochem.* **93**, 163–168 (1978).
 65. Oyama, N. & Anson, F. C. Facile Attachment of Transition Metal Complexes to Graphite Electrodes Coated with Polymeric Ligands. Observation and Control of Metal-Ligand Coordination among Reactants Confined to Electrode Surfaces. *J. Am. Chem. Soc.* **101**, 739–741 (1979).
 66. Frehill, F. *et al.* Microscopy and spectroscopy of interactions between metallopolymers and carbon nanotubes. *J. Phys. Chem. B* **109**, 13205–13209 (2005).
 67. Haas, O. & Vos, J. G. Preparation, characterisation and electrochemistry of electrodes coated with poly(4-vinylpyridine) bound ruthenium complexes. *J. Electroanal. Chem.* **113**, 139–149 (1980).
 68. Calvert, J. M. & Meyer, T. J. Poly(pyridyl)ruthenium(II) Complexes of Poly(4-vinylpyridine). Synthesis, Characterization, and Investigation of Optical and

- Electrochemical Properties. *Inorg. Chem.* **20**, 27–33 (1981).
69. Voss, M. E., Beer, C. M., Mitchell, S. A., Blomgren, P. A. & Zhichkin, P. E. A simple and convenient one-pot method for the preparation of heteroaryl-2-imidazoles from nitriles. *Tetrahedron* **64**, 645–651 (2008).
70. Sullivan, B. P., Calvert, J. M. & Meyer, T. J. Cis-trans isomerism in (trpy)(PPh₃)RuCl₂. Comparisons between the chemical and physical properties of a cis-trans isomeric pair. *Inorg. Chem.* **19**, 1404–1407 (1980).
71. Cheung, K.-C. *et al.* Ruthenium terpyridine complexes containing a pyrrole-tagged 2,2'-dipyridylamine ligand-synthesis, crystal structure, and electrochemistry. *Inorg. Chem.* **51**, 6468–75 (2012).
72. Manca, P. *et al.* Heteroleptic Ru(II)-terpyridine complex and its metal-containing conducting polymer: Synthesis and characterization. *Synth. Met.* **200**, 109–116 (2015).
73. Constable, E. C., Thompson, A. M. W. C., Tocher, D. A. & Daniels, M. A. M. Synthesis, characterisation and spectroscopic properties of ruthenium(II)-2,2':6',2''-terpyridine coordination triades X-ray structures of 4'-(N,N-dimethylamino)-2,2':6',2''-terpyridine and bis(4'-(N,N-dimethylamino)-2,2':6',2''-terpyridine)ruthenium(II). *New J. Chem.* **16**, 855–867 (1992).
74. Takeuchi, K., Thompson, M., Pipes, D. W. & Meyer, T. J. Redox and spectral properties of monooxo polypyridyl complexes of ruthenium and osmium in aqueous media. *Inorg. Chem.* **23**, 1845–1851 (1984).
75. Li, L., Wong, Y.-S., Chen, T., Fan, C. & Zheng, W. Ruthenium complexes containing bis-benzimidazole derivatives as a new class of apoptosis inducers. *Dalt. Trans.* **41**, 1138 (2012).
76. Hashiguchi, B. G., Young, K. J. H., Yousufuddin, M., Goddard, W. A. & Periana, R. A. Acceleration of nucleophilic CH activation by strongly basic solvents. *J. Am. Chem. Soc.* **132**, 12542–12545 (2010).
77. Lampman, P., Vyvyan, K., Pavia, D. L. & Kriz, G. S. *Introduction to spectroscopy*. (Cengage Learning, 2009).
78. Constable, E. C. Neo-classical coordination chemistry: Principles of ligand reactivity in coordination compounds. *Inorganica Chim. Acta* **145**, 49–51 (1988).
79. Blake, A. J. & Rankin, D. W. H. Structure of pyridazine at 100 K. *Acta Crystallogr. Sect. C Cryst. Struct. Commun.* **47**, 1933–1936 (1991).

80. Martinez-Carrera, S. The crystal structure of imidazole at -150°C . *Acta Crystallogr.* **20**, 783–789 (1966).
81. Garcia Velho, R. Medidas de condutividade na caracterização de complexos inorgânicos: um levantamento bibliográfico. Universidade Federal de São Carlos. (2006).
82. Geary, W. J. The use of conductivity measurements in organic solvents for the characterisation of coordination compounds. *Coord. Chem. Rev.* **7**, 81–122 (1971).
83. Huang, H., Zhang, P., Chen, Y., Ji, L. & Chao, H. Labile ruthenium (II) complexes with extended phenyl-substituted terpyridyl ligands: synthesis, aquation and anticancer evaluation. *Dalt. Trans.* **44**, 15602–15610 (2015).
84. Constable, E. C. & Hannon, M. J. Solvent effects in the reactions of 6-phenyl-2,2'-bipyridine with ruthenium(II). *Inorganica Chim. Acta* **211**, 101–110 (1993).
85. Thummel, R. P. & Jahng, Y. Polyaza Cavity-Shaped Molecules. 9. Ruthenium(II) Complexes of Annelated Derivatives of 2,2':6',2" - Terpyridine and Related Systems: Synthesis, Properties and Structure. *Inorg Chem* **25**, 2527–2534 (1986).
86. Scott, R. A. & Lukehart, C. M. *Applications of physical methods to inorganic and bioinorganic chemistry*. (Wiley, 2007).
87. Jakubikova, E. *et al.* Electronic Structure and Spectroscopy of $[\text{Ru}(\text{tpy})_2]^{2+}$, $[\text{Ru}(\text{tpy})(\text{bpy})(\text{H}_2\text{O})]^{2+}$, and $[\text{Ru}(\text{tpy})(\text{bpy})(\text{Cl})]^+$. *Inorg. Chem.* **48**, 10720–10725 (2009).
88. Bonnefous, C., Chouai, A. & Thummel, R. P. Cyclometalated complexes of Ru(II) with 2-aryl derivatives of quinoline and 1,10-phenanthroline. *Inorg. Chem.* **40**, 5851–5859 (2001).
89. Walba, H. & Isensee, R. W. Acidity Constants of Some Arylimidazoles and Their Cations. *J. Org. Chem.* **26**, 2789–2791 (1961).
90. Ford, P., Rudd, P., Gaunder, R. & Taube, H. Synthesis and Properties of Pentaamminepyridineruthenium(II) and Related Pentaammineruthenium Complexes of Aromatic Nitrogen Heterocycles. *J. Am. Chem. Soc.* **151**, 1187–1194 (1967).
91. Naskar, S. *et al.* Synthesis, characterization and theoretical studies of the heteroleptic Ruthenium(II) complexes of 2,6-bis(benzimidazolyl)pyridine. *Polyhedron* **100**, 170–179 (2015).

92. Corrêa, C. C. *et al.* Modified electrode using multi-walled carbon nanotubes and a metallopolymer for amperometric detection of L-cysteine. *Electrochim. Acta* **113**, 332–339 (2013).
93. Chetia, J. R., Moulick, M. & Dutta, A. Preparation, characterization and conductivity measurement of poly(4-vinyl pyridinium) salts in solid state. *Indian J. Chem. Technol.* **11**, 80–84 (2004).